NORTH ATLANTIC CARBON CYCLE RESPONSE TO CLIMATE VARIABILITY

by

David J. Ullman

A thesis submitted in partial fulfillment of

the requirements for the degree of

Master of Science

(Atmospheric and Oceanic Sciences)

at the

UNIVERSITY OF WISCONSIN-MADISON

2008

NORTH ATLANTIC CARBON CYCLE RESPONSE TO CLIMATE VARIABILITY

By David J. Ullman

Under the supervision of Professor Galen A. McKinley

ABSTRACT

Air-sea CO_2 flux variability in the North Atlantic has been found to be small in a variety of ocean biogeochemical models and at least one atmospheric CO_2 inversion study, yet the mechanisms that damp variability in this region of large net carbon uptake are poorly understood. A biogeochemical general circulation model was used to assess the impact of climate variability from 1980-2006 on the CO_2 flux and surface pCO_2 in the North Atlantic. Results show a strong correlation between flux and pCO_2 variability. Two distinct mechanistic regions are found explaining general pCO_2 variability: temperature driven versus dynamics (mixing) driven. Model output pCO_2 was separated into its influences from dissolved inorganic carbon (DIC), alkalinity (ALK), phosphate, silicate, sea-surface temperature (SST), and sea-surface salinity (SSS) to assess the mechanisms driving pCO_2 variability. These pCO_2 influences were regressed onto the North Atlantic Oscillation (NAO) index and onto the first principal component of the pCO_2 to assess the

effects of the main modes of climate and carbon variability in the region on the carbon system. The NAO regression shows that while the effects of SST and ALK on pCO_2 variability balance each other in the eastern subtropical gyre, DIC and SST effects balance in the subpolar gyre, such that the overall variability of pCO_2 is small. Regression of the pCO_2 components on the first PC shows that horizontal advection may also be important. Driving forces behind pCO_2 variability are evaluated with regard to limited data from transect and time series observations.

ACKNOWLEDGEMENTS

I would first like to thank my advisor, Professor Galen McKinley, for her guidance and encouragement. She embodies all the qualities of a great scientist, a fine role model for aspiring young researchers. I also thank her for encouraging me to diversify my education through participation in endeavors outside of the department.

The scientists and crew of the Roger Revelle on the CLIVAR I8S Cruise brought me immense inspiration for oceanography. Six weeks at sea provides for a dynamic learning environment through numerous discussions on the scope of such research. I would particularly like to thank Dr. Jim Swift and J.J. Becker for their guidance and generous support.

To my other thesis readers, Professor Eric DeWeaver and Professor Jack Williams, thank you for your helpful guidance. Your suggestions from outside of the field of oceanography helped enhance my understanding of the data from an outside perspective and challenged me to explain my findings to a general audience.

I would also like to thank Val Bennington. We struggled together to learn the inner workings of the model and data analysis in MATLAB, and without our discussions, I would have never made it through GFD II. I could not have asked for a better colleague.

I thank Dr. Stephanie Dutkiewicz for the many fresh ideas that she brought to this research. Her brainstorming visits were always most productive and encouraging. Also, her experience and knowledge of the model were particularly helpful in my research.

I would like to acknowledge Dierk Polzin for all of his help building hardware, setting up the compilers, and drafting scripts to run the model. Without his computing assistance, this project would not have gotten off the ground.

Finally, I would deeply like to thank my family and friends. Their lifelong love, support, advice, and humor have brought great balance to my life. All of you have provided with numerous opportunities for my life education and personal growth.

This research is funded by the National Aeronautics and Space Administration and Wisconsin Alumni Research Foundation. A special thanks goes to these sources and the Department of Atmospheric and Oceanic Sciences at the University of Wisconsin, Madison.

TABLE OF CONTENTS

Abstract i

Acknowledgements iii

Table of contents v

1. Introduction 1

    1.1 Ocean Carbon Cycle Chemistry 2

    1.2 North Atlantic Carbon Cycle Variability 5

    1.3 North Atlantic Climate Variability and the North Atlantic Oscillation 6

    1.4 Interannual Variability as a Path to Carbon Cycle Mechanisms . 7

2. Methods 8

    2.1 Model 8

    2.2 Sponge Layer 8

    2.3 Biogeochemical Model 9

    2.4 Model Spin Up 11

3. Results 12

    3.1 Model Validation: Gulf Stream Flow 12

    3.2 Mixed Layer Depths 14

    3.3 Interannual Variability of Mixed Layer Depths . . . 15

    3.4 Carbon Cycle Climatology 18

    3.5 BATS Carbon Cycle 19

4. Trends in North Atlantic Carbon Cycle Variability . . . 20

4.1 General Variability in pCO_2 and Influencing Parameters . 20

4.2 Temperature versus Dynamical Controls on Surface pCO_2 . 22

4.3 Mixing and the Vertical Supply of DIC 24

5. Carbon Cycle Response to Climate Variability 26

5.1 Calculation of pCO_2 Components 26

5.2 Regression of pCO_2 Components onto the NAO . . 27

5.3 Regression of pCO_2 Components onto the ENSO . . 28

5.4 Mechanisms driving pCO_2 variability related to the NAO . 28

5.5 Other Modes of Variability and EOF analysis . . . 31

6. Summary and Conclusions 35

6.1 Summary 35

6.2 Total Basin CO_2 Flux Variability 36

6.3 Future Work 38

References 41

Figures 47

1. INTRODUCTION

Since the Industrial Revolution, there has been a marked increase in the concentration of CO_2 in the atmosphere. Human activities, such as the burning of fossil fuels, the production of cement, and changes in land use, have all led to a change in atmospheric CO_2 concentrations from about 280 ppm in 1850 to values of about 380 ppm in 2007 (Keeling & Whorf, 2005). This increase, however, has been moderated through terrestrial and oceanic sinks that have assimilated roughly half of the total CO_2 emitted from anthropogenic sources (Sarmiento & Gruber, 2002). While the overall sink of anthropogenic CO_2 is primarily driven by the terrestrial biosphere, changes in land use and biomass burning have led to a terrestrial flux of CO_2 from the land to the atmosphere, such that the oceans have served as the only "true" sink for anthropogenic CO_2 over the past 200 years, and were it not for oceanic uptake, atmospheric CO_2 would be 55 ppm higher than present levels (Sabine et al., 2004).

The oceanic sink is an important factor in the long-term mean concentration of atmospheric CO_2, and it also exhibits a strong interannual variability. On the global level, the growth rate of atmospheric CO_2 varies considerably more than estimated anthropogenic CO_2 emissions (Conway et al., 1994, Sarmiento and Gruber, 2002), suggesting that interannual variability of CO_2 sinks have a strong impact on the overall variability in the atmosphere. For the ocean, year-to-year changes in climate forcing can have profound impacts on ocean temperature, chemistry, and circulation, all of which impact the ocean carbon cycle. Since atmospheric pCO_2 is nearly constant (yet increasing), air-sea flux variability is primarily driven by surface ocean pCO_2 variability. Aside from the prominent role of ENSO variability, the causes of interannual variability

in the mid to high latitude ocean sink is poorly understood, with estimates of sink magnitudes and variability largely inconsistent (McKinley et al., 2004; Gurney et al., 2002; Keeling et al., 1996; Peylin et al., 2005).

There is also significant spatial variability in the ocean sink. Due to differences in ocean circulation and chemistry, each basin has its own inherent ability to absorb atmospheric CO_2. The Atlantic Ocean plays a significant role in the uptake of anthropogenic CO_2. Takahashi et al. (2002) estimated that the Atlantic accounts for 41% of the global flux of CO_2 into the ocean. The North Atlantic (north of equator) is particularly important in the global CO_2 flux. While this basin comprises only 15% of the global ocean surface, it has absorbed 23% of the anthropogenic carbon stored in the oceans (Sabine et al. 2004).

1.1 Ocean Carbon Cycle Chemistry

The amount of CO_2 that fluxes into/out of the ocean is fundamentally driven by the difference between the partial pressures of CO_2 in the surface ocean and the atmosphere ($\Delta pCO_2 = pCO_2 ocean - pCO_2 atm$). If the pCO_2 in the atmosphere is higher relative to the surface ocean, then the net flux of CO_2 will proceed from the atmosphere to the ocean, and vice-versa. In other words, regions where $\Delta pCO2<0$ are considered undersaturated waters and regions with $\Delta pCO_2>0$ are considered supersaturated. Since $pCO_2 atm$ is relatively constant in space due to rapid atmospheric mixing (yet increasing over time), spatial variability in ΔpCO_2 is driven by changes in surface ocean pCO_2.

Other controls on surface ocean pCO_2 include changes in temperature, salinity, alkalinity (ALK), and dissolved inorganic carbon (DIC). For a given pCO_2 (salinity,

ALK, and DIC held constant), Takahashi et al. (1993) experimentally found the following relationship to explain the connection between temperature and pCO_2:

$$\frac{1}{pCO_2}\frac{\partial pCO_2}{\partial T} = \frac{\partial \ln pCO_2}{\partial T} \approx 0.0423^{\circ}C^{-1}$$

Thus, an increase in SST causes an increase in sea surface pCO_2. A similar directly proportional relationship exists for salinity, but does not have as strong an impact on pCO_2 as temperature.

After dissolving into ocean water, CO_2 acts as an acid/proton donor to form H^+, HCO_3^-, and CO_3^{2-} according to the following chemical equation (where $H_2CO_3^*$ is the pre-dissociation dissolved CO_2):

$$H_2O + CO_2(g) \Leftrightarrow CO_2(aq) \Leftrightarrow H_2CO_3^* \Leftrightarrow H^+ + HCO_3^- \Leftrightarrow 2H^+ + CO_3^{2-}$$

The variable used to describe the overall state of this carbon cycle is dissolved inorganic carbon (DIC), which is defined as the sum of the concentrations of all dissolved carbon species, or:

$$DIC = [H_2CO_3^*] + [HCO_3^-] + [CO_3^{2-}]$$

Clearly, as DIC increases, the overall amount of carbon in the system increases, along with pCO_2, so regions with elevated DIC will exhibit a decreased (or reverse/outgassing) air-sea flux.

Another chemical property of seawater that affects the pCO_2 near the surface is alkalinity (ALK). Alkalinity is defined as the measure of the excess of bases over acids (Sarmiento and Gruber, 2006) and is often best understood by the following equation:

$$ALK = [HCO_3^-] + 2[CO_3^{2-}] + [OH^-] - [H^+] + [B(OH)_4^-] + \text{minor bases}$$

Clearly there is some relationship between DIC and ALK through the carbonate and bicarbonate ions, and hence ALK is also an important property defining the chemical balance of the carbon in seawater. However, DIC and ALK affect pCO_2 in different ways (where k0, k1, k2 are chemical equation rate constants):

$$pCO_2 \approx \frac{k2}{k0 \bullet k1} \bullet \frac{(2 \bullet DIC - ALK)^2}{ALK - DIC}$$ (Sarmiento and Gruber, 2006).

The equation above shows the directly proportional relationship between DIC and pCO_2 and an inversely proportional relationship between ALK and pCO_2.

The physical carbon cycle is further complicated through the effects of temperature on surface ocean dynamics. As discussed above, changes in ocean temperature have an immediate impact on the pCO_2 of the surface ocean, with colder waters less able to hold pCO_2. However, colder waters are also denser, driving increased mixing which brings high DIC waters from depth to the surface to balance a required conservation of mass, thus increasing pCO_2. (Deep waters are typically higher in DIC from the accumulation of carbon sinking through the "biological pump," discussed next). These opposing impacts on the surface pCO_2 drive some regions to be dominated by mixing (dynamics-driven) and other regions dominated by temperature (temperature driven).

The discussion thus far describes the inorganic carbon cycle pathway, and while the focus of this thesis is not on the biological uptake of CO_2, it is important to note that biological processes can have regionally large impacts on the distribution of carbon. Through photosynthesis, carbon is incorporated into biological material at or near the surface. This biological material can be remineralized (i.e. redissolved) into surface

waters, transported downward and remineralized at depth, or transported to the seafloor and incorporated into sediments. The downward transport removes DIC from the surface, and the subsequent remineralization below the mixed-layer drives the high concentrations of DIC in the deep ocean. This downward transport of carbon is referred to as the "Biological Pump."

1.2 North Atlantic Carbon Cycle Variability

While the overall uptake of CO_2 by the North Atlantic has been found to be relatively important on a global scale, the significance of North Atlantic flux variability is less clear. Atmospheric inverse models (Bousquet et al., 2000) and spatially extrapolated timeseries data (Gruber et al., 2002) suggest North Atlantic flux variability range to be on the order of ±0.3 Pg C $year^{-1}$, a significant fraction of the global ocean CO_2 flux variability of ±0.5-1.0 Pg C $year^{-1}$ (Le Quéré et al., 2000; Bousquet et al, 2000). Other forward modeling studies, however, have suggested that global ocean flux variability is smaller (less than ±0.5 Pg C $year^{-1}$) and that the North Atlantic does not play a significant role in this variability (McKinley et al., 2004; Obata and Kitamura, 2003; Le Quéré et al., 2000). Biogeochemical ocean models do tend to under-represent surface physical variability (McKinley et al., 2004; Peylin et al., 2005; Le Quéré et al., 2000), but even if one assumes forward model output to be a lower bound, there is still a discrepancy in the understanding of flux variability in the North Atlantic.

1.3 North Atlantic Climate Variability and the North Atlantic Oscillation

The prominent mode of climate variability in the North Atlantic region is the North Atlantic Oscillation (NAO). The NAO is a redistribution of atmospheric mass between the Subtropical and Northern North Atlantic (Hurrell & Dickson, 2004). It is most often operationally defined as the difference between surface pressures of the Azores high-pressure center and the Icelandic low-pressure center. Most pronounced during Northern Hemisphere winter months, the variability in this meridional pressure gradient drives significant climate variability in the atmosphere and the underlying ocean, accounting for one-third of the variance in sea level pressure over the North Atlantic (Hurrell et al., 2003). During a positive phase of the NAO, a large meridional pressure gradient drives a number of climatic changes: enhanced westerly flow bringing warm moist air across the mid-North Atlantic and into Europe, enhanced warm southerly flow over the eastern United States, and enhanced cold northerly flow over Greenland and the western Atlantic (Hurrell et al., 2003). Such anomalous flow drives a northeastward shift in Atlantic storm activity, with more intense and frequent storms near Iceland and the Norwegian Sea (Hurrell et al., 2003).

These changes in atmospheric climate have an impact on surface ocean variability. Most pronounced is the typical tripole pattern of the leading mode of SST variability in the North Atlantic, with anomalously cold SST in the subpolar region, anomalously warm SSTs in the mid-latitude Atlantic off of Cape Hatteras, NC, and anomalously cold SSTs between 0-30˚N (Visbeck, 2001). Due to the strong link between surface wind and surface ocean circulation, numerous studies have also shown significant impacts of the NAO on ocean circulation (Bersch, 2002; Marshall et al., 2001). Finally,

changes in atmospheric circulation and pressure associated with the NAO influences overall storminess and precipitation over the ocean (Bojariu and Reverdin, 2002; Mariotti and Arkin, 2007). Such changes in cloud cover and freshwater input have a strong impact on surface salinity, temperature, and alkalinity (Mignot and Frankignoul, 2003).

1.4 Interannual Variability as a Path to Carbon Cycle Mechanisms

This thesis aims to understand the effects of interannual variability in atmosphere and ocean physics on the North Atlantic carbon sink. Looking at interannual variability is useful because it can aid in developing an understanding of the mechanisms that drive the ocean carbon cycle. A mechanistic understanding of ocean carbon cycle will allow for better prediction of future change in an environment of increasing atmospheric CO_2.

Through the use of the MIT ocean-biogeochemical general-circulation-model, the effects of climate variability from 1980-2006 on the air-sea flux of carbon and surface pCO_2 in the North Atlantic is assessed. Since the NAO is the main mode of variability within the North Atlantic, this well-known index of climate variability is used to help interpret variability in the model output. Other modes of ocean pCO_2 variability that arise through other climate variability are also discussed using Empirical Orthogonal Functions (EOFs) also known as Principal Component Analysis (PCA). This analysis helps indicate other mechanisms driving carbon cycle variability aside from those due to changes in the NAO.

2. METHODS

2.1 Model

The MIT Ocean General Circulation Model (Marshall et al., 1997a,b) was regionally configured for the North Atlantic between 20˚S and 81.5˚N, with a horizontal resolution of 0.5˚ latitude and 0.5˚ longitude. The model is set up to have 23 vertical levels with a resolution of 10 m thickness at the surface increasing to 500 m thickness for depths greater than 2200 m. The Gent-McWilliams (Gent & McWilliams, 1990) eddy parameterization and the KPP boundary layer mixing scheme (Large et al., 1994) are employed to represent sub-gridscale processes. The general circulation model is forced with daily wind stress (10 m), net heat flux (Qnet), and freshwater (evaporation minus precipitation or EmP) flux, using 1980-2006 reanalyzed output from the National Centers for Environmental Prediction (NCEP) reanalysis I (Kalnay et al., 1996).

2.2 Sponge Layer

To address rigid boundary issues in this regional model, a "sponge layer" is included to dampen accumulation of tracers along false boundaries that would in reality flow out of the North Atlantic into other ocean basins. A sponge layer acts to relax values along the boundary to climatological values, such that grid cells closest to the boundary have the biggest weight, with influence dropping off away from the boundary as described by the following equation:

$$\frac{\partial(tracer)}{\partial t} = \frac{\partial(tracer)}{\partial t} - \lambda \frac{(tracer - tracer\_obs)}{\tau_{RELAX}},$$

where applied values of λ decrease nearly exponentially away from the boundary, *tracer_obs* is based on monthly climatological values, and τ_{RELAX} is the relax timescale (how often the model relaxes back to climatology). The decrease in λ away from the boundary results in a stronger forcing back to the climatology for grid cells closer to the boundary and a weaker relaxation back to the climatology away from the boundary (thus a bigger influence by model dynamics). For temperature and salinity, the sponge layer is implemented along the southern boundary and at the Mediterranean inflow of the Strait of Gibraltar. For nutrients of the biogeochemical model, the sponge layer is only implemented along the southern boundary. Attempts were made to include a sponge layer along the northern boundary (north of 81.5˚N), but tests comparing the effects on circulation, temperature, and salinity show that a sponge layer along this boundary is inconsequential and therefore can be discarded. Similarly, differences in biological production between the Mediterranean and the eastern basin are small, suggesting that nutrient inflow from the Mediterranean is insignificant (Béthoux et al., 1998). Therefore the nutrient sponge layer at this boundary was not included.

2.3 Biogeochemical Model

Also included in the total model is an ecosystem model of intermediate complexity (Figure 1) as developed by Dutkiewicz et al. (2005), modeling a pelagic ecosystem with one zooplankton class and two phytoplankton classes: diatoms and "small" phytoplankton. This ecosystem is limited by the coupled cycles of phosphorus, silicon, and iron. Biological iron cycling is modeled following Parekh et al. (2004), using an aeolian dust input (Mahowald et al., 2003; Luo et al., 2003). The phytoplankton classes

differ in their maximum growth rate, nutrient requirements, and edibility by the zooplankton (the larger diatoms are less palatable). The small phytoplankton are limited by phosphorus and iron only, but the diatoms are limited by phosphorus, iron, and silicon. Nitrogen cycling is not incorporated because of its higher complexity and because it is less of a limiting nutrient in the North Atlantic than in other basins (Sarmiento & Gruber, 2006). Both phytoplankton classes are also limited by light, prescribed in the model by defining the photosynthetically available radiation (PAR) as a percentage of the amount of shortwave radiation reaching the surface ocean (from NCEP forcing). PAR decreases vertically in water column factoring attenuation coefficients for the water itself and the biological abundance increasing the turbidity. During winter months, the amount of light reaching the surface is also dependent on the amount of ice cover (assuming high-albedo ice cover blocks shortwave radiation from reaching the upper ocean). This ice-cover is also prescribed by data from the NCEP reanalysis I (Kalnay et al., 1996).

While the ecosystem is confined to the surface layers, nutrient cycles are computed over the entire water column. Nutrients are carried in the modeled plankton species and through pools of particulate organic matter (POM) and dissolved organic matter (DOM). Both zooplankton and phytoplankton contribute to the pools of DOM and POM, but among phytoplankton, diatoms contribute more to POM due to their larger size. While DOM remains suspended in the water column, POM sinks at a constant rate, simulating the "biological pump" of organic matter and nutrients to the abyss. Both POM and DOM are affected by ocean circulation and remineralize into an inorganic and bio-available pool of nutrients. Nutrients at depth can be recirculated to the surface through advection and convective upwelling.

Carbonate chemistry is modeled using values of DIC, ALK, phosphate, silicate, temperature, salinity, and pH to calculate the surface pCO_2 (Follows et al., 2006). The air-sea gas exchange for CO_2 is modeled as a function of temperature, the square of the wind-speed, and the difference between pCO_2 in the surface water and pCO_2 in the atmosphere following relationships described by Wanninkhof (1992). Atmospheric pCO_2 levels were prescribed following the time-varying curve from Mauna Loa observations (Keeling & Whorf, 2005), which include the seasonal cycle and the increasing trend over time. Changes in carbon and oxygen due to changes in biology are calculated using the fixed Redfield ratio, expressing the ration between oxygen, carbon, silicate, and phosphorus as 170:120:25:1 (Anderson & Sarmiento, 1994).

2.4 Model Spin Up

The physical model was spun up through three 27-year cycles of varying daily forcings from 1980-2006 (total of 81 years spin up). In order to curb drift throughout the spin up, potential temperature and salinity were relaxed back to climatology from the World Ocean Atlas (WOA, Locarnini et al., 2006; Antonov et al., 2006) on timescales of every 2 and 4 weeks respectively. This relaxation to climatology reduces the overall variability in the model output but aids in the reduction of unrealistic model drift.

Next, the biogeochemical model was spun up for ten years of 1980-1989 daily forcing with a constant atmospheric pCO_2 fixed at 345 ppm (roughly the 1980 level) with temperature/salinity relaxation included as before. This spin up was repeated for another 10 years with the same forcing to eliminate any drift still in the biogeochemical system after the first 10 years.

During the last 27-year cycle of the spin up, the relaxation terms (i.e. modeled value minus climatological value, or the amount that the model uses to correct back to climatology at each time step) were extracted from the output. A daily climatology of these relax terms was created from the 27-years of output. This relaxation climatology was then incorporated back into the forcing files of net heating and freshwater fluxes (Qnet+Trelax; EmP-Srelax). In this way, the relaxation needed to keep the model stable was incorporated into the forcing itself so that the relaxation step could be eliminated and the overall variability enhanced (no longer limited each time step by the relaxation). Preliminary tests of this method show that temperature and salinity in the model do indeed remain relatively stable, but the overall variance in the data increases appreciably, which is advantageous when studying interannual variability in the ocean system. Figure 2 shows the seasonal cycle and anomalies from a ten-year test run to compare output with the relaxation turned on versus output with relaxation terms incorporated into the forcing. While there are small differences in the overall mean cycle, there is a considerable increase in the overall variability present in the anomalies when the relaxation is turned off. The final run used the full biogeochemical model with relaxation turned off, 1980-2006 daily forcings that incorporated the climatology of the relax terms, and the time-varying atmospheric pCO_2 field.

3. RESULTS

3.1 Model Validation: Gulf Stream Flow

One of the main reasons for modeling the ocean is due to a lack of observational data. To empirically sample the ocean with the spatial and temporal resolution to competently

assess its complex mechanisms would be so prohibitively expensive, it would be impossible. Models help to fill in the gaps of the puzzle where the pieces are unavailable. The limited data that is available, however, is necessary to validate that the model is within the realm of reality. (Of course, the acquisition of more data always helps to further constrain the models, adding more pieces to the puzzle and shrinking the gaps to be filled in by the model).

Table 1: Transport comparisons in Sverdrups (1 Sv = 10^6 m^3/s)

LOCATION	MODEL	OBSERVED	SOURCE
Gulf Stream at Cape Hatteras	50.6 Sv	70-100	Tomczak and Godfrey (1994)
Gulf Stream at 65˚W	28.6 Sv	90-150 Sv	Tomczak and Godfrey (1994)
Gulf Stream at 40˚W	20.9 Sv	37 Sv	Worthington (1976)
Florida Strait at 26.5˚N	15.0 Sv	31.5 Sv	Cunningham et al. (2007)
Florida Strait at 26.5˚ N (extended)	26.3 Sv		

Table 1 compares the model transport of major ocean currents in the North Atlantic with published observations. All of the Gulf Stream model estimates integrate the current velocity over a span of 15˚ wide and 985m deep to calculate the transport. All estimates of the Gulf Stream are considerably less than the observed estimates. It appears as though the model is poorly representing the recirculation in the north, a characteristic problem for the MITgcm and similar non-hydrostatic models (McKinley et al, 2000). Such recirculation would intensify the western boundary current.

Upon further investigation of the location of the Gulf Stream, our model shows a northward displacement of the location of the Gulf Stream relative to observation.

Because the initial spin up relaxes to the observational mean of temperature and salinity, this relaxation may also cause a damping of the transport in this current.

The Florida Strait is typically strong and narrow current confined between the coast of Florida and the Bahamas. Because our model does not resolve the Bahaman Islands, some of this flow in the model extends past the width of the observed width of the Florida Strait. If the extended width of the flow is included in the calculation ("extended" estimate, in Table 1), then the modeled transport compares favorably with the observations.

3.2 Mixed Layer Depths

Another way to measure the overall skill of a physical ocean model is to look at its mixed layer depths (MLDs). MLD is dependent on the density stratification of the ocean and thus a function of salinity (S) and temperature (T). Comparing MLDs between model results and observations is useful because it integrates both of the physical parameters affecting density. MLD is also a crucial variable for comparison due to its importance with regard to the carbon cycle. Changes in MLD can affect the amount of DIC and nutrients reaching the surface, and MLDs are driven in part by changes in T, all of which affect the air-sea carbon flux. For the purpose of this study, MLDs have been calculated as the depth at which potential density exceeds that of the surface by 0.125 kg/m^3 (following Monterey & Levitus, 1997).

Figure 3 compares seasonal MLD output from the model with observed climatology from the WOA database (MLD calculated from salinity and temperature climatology; Locarnini et al., 2006; Antonov et al., 2006). The model captures the

magnitude and spatial distribution of mixing fairly well, particularly in summer months, when the water column is more stratified. During the winter months, however, the model overestimates deep mixing in high latitude regions such as the Norwegian Sea and the waters off the southern coast of Greenland. Much of this has to do with high variability in regions of deep winter mixing, but the depth resolution of this model is also coarse below 1000m depth (up to 500m resolution), such that small changes in the temperature/salinity structure can result in significant MLD overestimates. Also, the observational record of these high latitude regions is more limited in winter months due to rough seas and sampling difficulty, suggesting that there may be a higher degree of uncertainty in the climatological estimates of MLDs in the North Seas.

The seasonal climatology comparisons of MLD also highlight differences in the location of the Gulf Stream. This difference is particularly strong in the winter months with evidence of a weaker Gulf Stream. This weaker transport of warm subtropical waters limits the warming of these waters off of Newfoundland, which subsequently drives relatively deeper mixing in the model. The MLD differences near the Gulf Stream in the summer months shows a dipole of deeper/shallower MLDs, suggesting a displacement in the location of the Gulf Stream between the model and observations, with the location of the model's Gulf Stream displaced southward (light blue regions, centered at approximately 35˚N, 60˚W in Figure 3).

3.3 Interannual Variability of Mixed Layer Depths

There is a limited observation record of MLD variability available from the Bermuda-Atlantic Timeseries Station (BATS, 31˚40”N, 64˚10”W, [Bates, 2007]), providing

monthly-resolved Conductivity-Temperature-Depth (CTD) instrument data since 1988. The model matches the observed seasonal climatology at BATS quite well (Figure 4), with an overestimate of about 50m during February and March, times of deep mixing. Comparing the MLD variability shows that the timing of the mixing in the model also matches the data, but the magnitude of the winter mixing in the model goes from too shallow in the early 1990s to too deep in the 2000s. There appears to be a deepening trend in the model MLDs over the time period from 1991 to 2006, while the observations appear to have the opposite trend.

Because MLDs in the BATS region are mostly temperature dependent (this demonstrated in T dependence on MLD over seasonal time scales), it is useful to look at temperature independently of salinity to understand what might be causing this trend in our model results. More interannual varying SST data is available from satellite observations since the early 1990's. The Pathfinder program uses an Advanced Very High Resolution Radiometer (AVHRR) to measure the skin temperature (upper 1mm or less) of the ocean (Kilpatrick et al., 2001). The model dynamics, however, deal with a layer of the upper 10 m of the ocean. Since the skin temperature heats up much more rapidly than the upper 10 m during the exposure to daytime shortwave forcing, nighttime satellite measurements are ideal when trying to compare Pathfinder SST with the model SST. The Pathfinder data is useful because it provides SST variability from 1985 to the present. Even with nighttime data, however, one must be mindful that these measurements reflect the skin temperature only and not the temperature of a layer of water with any kind of considerable depth. To get around such issues, Reynolds and

Smith (1994) developed an algorithm to correct satellite data to account for temperature in the upper 10 m as opposed to that confined to the skin layer.

To look at the model's ability to capture SST at BATS, Figure 5 compares SSTs as measured by the BATS timeseries, Pathfinder nighttime skin temperature, the Reynolds algorithm, and model output. The Pathfinder and Reynolds measurements match those at BATS quite well, with some negative bias by Pathfinder for winter SST, which is consistent with the understanding of a thermally responsive nighttime skin temperature. This plot confirms that the model SSTs are too warm in the early 1990's and too cold in the end of the run, i.e. a decreasing trend. Since colder surface water helps to drive deeper mixing, these differences in SST probably are driving the anomalously deep MLDs in the model.

But what is causing this anomalous negative SST trend in our model? The net heating forcing (Qnet) in the model has the most direct impact on surface temperature. Figure 6 shows the decreasing trend in annually-averaged Qnet (negative values indicate loss of heat from atmosphere forcing, thus cooling of ocean surface) in line with the cooling effect in SST (R=0.61; lag-1 year R=0.66). The change in Qnet from the early 1990's to the late 2000's amounts to about -23.8 W m^{-2}. This decrease in Qnet acting over a column of water with depth 200 m for 5 years would result in a decrease in SST of 4.4˚ C. The decrease in SST observed in the model at BATS over the same time period is roughly 4.0˚ C.

Clearly the cooling trend in modeled SST is responding to a trend in the net heat flux forcing. For some reason however, this trend is not manifest in the observations, suggesting that the model is missing an important warming mechanism needed to

accurately model SSTs in the region around BATS by offsetting the cooling caused by the atmospheric forcing. The two mechanisms driving SST change at BATS are the net heating and any form of heat convergence from transport into the region. It is possible that the NCEP Qnet term is incorrect for this region, but it is more plausible that the model may not be capturing the heat convergence. This hypothesis is supported by the underestimate of recirculation/transport along the Gulf Stream north of Cape Hatteras (discussed above). Perhaps the act of restoring to an invariant WOA climatology along the southern boundary limits the variation in global meridional overturning circulation (Zhang et al., 2007), thus limiting the advection of warm equatorial water that would otherwise compensate for the atmospherically forced cooling. This as an important limitation in the model results that leads to a significant caveat in the findings of this thesis. Because of these discrepancies, our model is able to show the effect of the atmospheric forcing within the North Atlantic, but overall patterns in the real world may be damped by mechanisms not included in the model. Nevertheless, a better understanding of the links between the atmospheric forcings and the ocean is still useful information in understanding the overall picture in the ocean carbon cycle.

3.4 Carbon Cycle Climatology

Since the focus of this thesis is ultimately on the carbon cycle, it is useful to compare surface pCO_2 observations with the model output. As shown by Takahashi et al. (1993), pCO_2 values can be separated into temperature-driven and non-temperature-driven components. Figure 7 compares modeled seasonal pCO_2 differences with climatological observations (Takahashi et al., 2002) by showing the overall pCO_2 and its temperature

and non-temperature components for model output and observations. The model is able to capture much of the spatial variability in the total pCO_2 seasonality. The model shows the characteristic total seasonal pCO_2 difference tri-pole pattern of similar magnitude as seen in the observed climatology. Despite the inaccuracies in mean SST related to potential issues of heat flux convergence the model, the model does particularly well in describing the climatological temperature component of the pCO_2. However, the model does not seem to fully capture the non-temperature component in the subtropics, due to underestimation of biological activity in these oligotrophic waters, a problem common to this type of model. Any inaccuracies in the overall pCO_2 field are driven by discrepancies in the non-temperature component of the pCO_2, but despite these shortcomings, the model is doing reasonably well in capturing the mean seasonal cycle of pCO_2 and its components (Bennington et al., in prep), a challenging task as illustrated by recent work in the North Pacific (McKinley et al., 2006).

Aside from a few limited timeseries data sets, these climatological observations are the only carbon data available for the global oceans. Complete verification of the carbon cycle is restricted because of the lack of variability data, but indeed, this is a key reason for modeling the carbon cycle.

3.5 BATS Carbon Cycle

One timeseries for DIC and pCO_2 has become available from 1983 through 2006 at Bermuda (Bates, 2007). The modeled pCO_2 matches the observed timing of the seasonal cycle, but the modeled summer magnitudes overestimate observations for most of the timeseries (Figure 8a). These results are related to the temperature and DIC controls on

pCO_2. As discussed in 3.3, modeled summer SSTs are too high for the time period of 1990 to 2000 (Figure 8b). After 2002, summer and winter SSTs are low with respect to observations. These aberrations in temperature have a direct impact on pCO_2 for 1990-2000, as summer pCO_2 is related to the elevated SSTs.

During 1990-2000, modeled DIC matches the timing of the seasonal cycle with some overestimation of summer DIC (Figure 8c), most likely related to the biological cycle (Bennington, in prep.). These differences in DIC summer magnitude combine with high SSTs to create a significant overestimate of summer pCO_2. After 2002, mean model DIC is consistently higher for all seasons. This elevated DIC offsets the low SST during this period, resulting in a pCO_2 curve that matches observations. A similar relationship exists before 1990. The model appears to be correctly capturing the total pCO_2 variability, but it does so for the wrong reasons, with opposing inaccuracies in temperature and DIC.

4. TRENDS IN NORTH ATLANTIC CARBON CYCLE VARIABILITY

4.1 General Variability in pCO_2 and Influencing Parameters

As described in the introduction, the pCO_2 of the surface ocean is influenced by a number of factors. Many of these factors have opposing impacts on pCO_2, such that an understanding of what drives the overall pCO_2 variability is far from straightforward. In order to better understand the interannual variability in the results, all of the data has been linearly detrended and deseasonalized (using a 12-month smoother). Such steps remove seasonal variability and any trends in the data, such as increases in SST or anthropogenic carbon. The remaining variability is considered the interannual variability in the system.

Although the CO_2 flux is most relevant for understanding the variability of the ocean as a carbon sink, this analysis will focus on pCO_2 as the carbon variable of choice because SST, DIC, and ALK directly impact pCO_2. Aside from the difference in pCO_2 between the air and the sea, the only other parameter to impact the CO_2 flux is the square dependence of the wind speed/stress (Wanninkhof, 1992). However, other analyses have shown wind variability has a small impact on the flux variability and that the flux variability is mainly driven by patterns in pCO_2 variability (Takahashi et al., 2002; McKinley et al., 2006; Bates, 2007; Omar et al., 2007)

To assess the main modes of variability within the carbon system, a principal component analysis (PCA) was conducted on the pCO_2 and CO_2 flux output to determine the first empirical orthogonal function (EOF1) and associated principal component (PC1) over 1981-2006 (first year of variability removed as a shock year). The first EOFs of pCO_2 and CO_2 flux explain similar amounts of the overall variance (32% and 26%, respectively) and show similar spatial patterns (Figure 9a, b), suggesting that much of the flux variability is driven by similar variability in the pCO_2. Therefore, the surface pCO_2 can be used as the main driver to describe the CO_2 flux. As seen from Figure 9c, this choice is acceptable as the main modes of temporal variability in pCO_2 and the CO_2 flux (i.e. the PC1s) are highly correlated ($r=0.97$).

For an initial sense of the overall variability in the carbon cycle and to see what is driving this variability in a first order approximation, it is useful to look at the standard deviation of the surface pCO_2 and the variables effecting carbon chemistry in the surface ocean (SST, surface DIC, and ALK). As seen from the standard deviation of pCO_2 (Figure 10a), high variability is seen in the subtropical gyre, particularly centered at two

locations in the eastern and western sides of the basin along 30˚N, with the highest variability located in the western subtropical gyre. Incidentally this bulls-eye of heightened variability is near BATS (31˚40”N, 64˚10”W), suggesting the importance of this timeseries in understanding a location of high pCO_2 variability in the North Atlantic. The eastern region of high pCO_2 variability is roughly centered at 10˚N, 25˚W.

These locations of high pCO_2 variability appear to be collocated with regions of high SST variability (Figure 10b), suggesting the importance of temperature variability driving pCO_2 variability in these regions. The center of moderately high pCO_2 variability in the eastern subtropics (roughly 30˚N, 25˚W) is also collocated with enhanced variability in surface ALK (Figure 10d). Since temperature and ALK affect pCO_2 in opposing directions, the ALK variability appears to damp the effect of SST variability on the overall pCO_2 variability at this location.

There is also high variability in the surface DIC and ALK fields (Figures 10c and 10d) in the western tropics (roughly 15˚N, 60˚W) and near the Grand Banks (45˚N, 50˚W). This high variability, however, does not appear to manifest in the overall pCO_2 variability. As discussed in the introduction, DIC and ALK also have opposing impacts on pCO_2, and the locations of high standard deviation in DIC and ALK are collocated, suggesting that the effects of large DIC and ALK variability on overall pCO_2 variability have a canceling effect on each other.

4.2 Temperature versus Dynamical Controls on Surface pCO_2

By correlating various surface parameters in the North Atlantic from model output, some general trends in the carbon cycle’s response to ocean physics become apparent.

Following the argument of LeQuéré et al. (2003), the two major physical controls on surface ocean pCO_2 are temperature and dynamical mixing. For example, increased mixing brings older DIC-rich waters to the surface to drive an increase in pCO_2, but this increased mixing is also related to lower SST, driving a decrease in the pCO_2. Much of pCO_2 variability is dominated by one or the other of these controls (temperature vs. dynamics), as can be seen from the correlation of pCO_2 and SST (Figure 11a). Regions exhibiting a negative correlation between pCO_2 and SST are considered "dynamics-dominated," such that a decrease in SST drives an increase in mixing, bringing more DIC to the surface, and thus increasing the pCO_2. Regions exhibiting a positive correlation are "temperature-dominated," such that an increase in SST directly forces an increase in pCO_2 through the thermodynamic controls on gases in seawater. Regions exhibiting zero correlation are neither temperature- nor dynamics-dominant. As seen in Figure 11a, the dynamics-driven controls on pCO_2 are confined to the subpolar gyre, and temperature-driven controls dominate the entire basin south of 45˚N (consistent with the findings of LeQuéré et al., 2003).

That the carbon cycle is driven by dynamics in the subpolar gyre is consistent with the deep mixing of this region (see MLD plots in Figure 3). Subpolar SST cooling drives mixing that is much deeper than in much of the rest of the North Atlantic, driving the upwelling of DIC-rich waters to alter pCO_2 more than by the gas solubility effects due to changes in temperature. Figure 11b shows that the subpolar pCO_2 is indeed positively correlated with deeper mixing, and this mixing draws increased DIC to the upper 100m. South of 45˚N, temperature dominates the surface pCO_2, resulting in a negative correlation between pCO_2 and DIC (Figure 11c) that would otherwise be

counterintuitive. Finally, the correlation between the Air-Sea CO_2 flux and MLD show that changes in mixing dominate the CO_2 flux in the subpolar gyre, but the subtropical CO_2 flux is driven by opposing temperature effect (Figure 11d). (Note: comparing Figures 11b and 11d also show the strong negative correlation between CO_2 Flux and surface pCO_2).

4.3 Mixing and the Vertical Supply of DIC

In general, deeper mixing brings more DIC to the surface, and thus MLD is typically positively correlated with the vertical supply of DIC. In the real world, it can be difficult to measure the vertical supply of DIC, but the model is useful because it can calculate this term at each time step as the amount of DIC that is transported vertically between grid cells.

Upon looking at the correlation between MLD and the DIC vertical supply (Figure 12a), the relationship between the two parameters is not so straightforward. Instead of the correlation being strongly positive across the entire basin, there are localized regions that show a negative correlation (south of 15˚N and eastern subtropical gyre centered at 25˚N, 40˚W). Depth profiles of DIC for winter and summer months (Figures 12c and 12d) show that unlike other locations in the ocean where DIC is at a minimum within the mixed layer, the eastern subtropical gyre location (green profile) shows a negative vertical gradient of DIC in the surface layer above 100m (particularly strong in summer), such that deeper mixing taps into lower concentrations of DIC, reducing the overall concentration of DIC vertically supplied to the surface, thereby driving the negative correlation between MLD and DIC vertical supply. This profile

seems to indicate heightened productivity and uptake of DIC below the immediate surface layers related to the existence of a subsurface chlorophyll maximum, common in subtropical waters (Mann & Lazier, 1996).

The region south of 15˚N, however, does not show the same DIC minimum at depth to suggest the same mechanism of the negative correlation between MLD and DIC vertical supply (black profile in Figures 12c and 12d). Instead, this negative correlation appears to be related to the vertical velocity of this region (Figure 12b). Vertical velocity is highly correlated with DIC vertical supply, suggesting that the vertical velocity drives the vertical supply of DIC more than the mixing. In this region, vertical transport supplies DIC to the surface layer while pushing denser waters upward, causing an increase in the stratification of surface waters and a shoaling of the MLD (upwelling prohibits mixing). In this way, MLDs are negatively correlated with DIC vertical supply.

This regional analysis of the relationship between MLD and DIC vertical supply shows that values of subsurface parameters can have a profound impact on surface carbon chemistry when using a time-varying 3-D model. A 2-D box model, for instance may only consider one type of DIC vertical profile, leading to the basic understanding of a DIC minimum at the surface. This model, however, helps to demonstrate that more complicated states of DIC vertical distribution can indeed exist.

While the strong negative correlation between MLD and DIC vertical supply exists in the eastern subtropical gyre, however, the effect of this subsurface chlorophyll maximum on the total carbon cycle of the region is small. The negative gradient in DIC is consistent such that it drives the negative correlation, but it is small in magnitude, with the summer DIC subsurface minimum only 10 mmol/m^3 less than surface values

(pertaining to a percent difference in DIC concentration of less the 0.5%). Similarly, MLDs in this region and areas south of 15˚N are consistently small throughout the year (Figure 3), such that upwelling-induced changes in the MLD do not cause a great impact in the depth of mixing. Overall, the existence of these negative correlations between MLD and DIC vertical supply has a small effect on the overall CO_2 flux variability of the basin.

5. CARBON CYCLE RESPONSE TO CLIMATE VARIABILITY

5.1 Calculation of pCO_2 Components

As described by Takahashi et al. (1993), pCO_2 of the surface ocean can be separated into influences from DIC, Temperature (T), ALK, Salinity (S), Phosphate (PO4), and Silicate (SIL) according to the following equation:

$$\frac{dpCO_2}{dt} = \frac{\partial pCO_2}{\partial DIC}\frac{dDIC}{dt} + \frac{\partial pCO_2}{\partial SST}\frac{dSST}{dt} + \frac{\partial pCO_2}{\partial ALK}\frac{dALK}{dt} + \frac{\partial pCO_2}{\partial S}\frac{dS}{dt} + \frac{\partial pCO_2}{\partial PO_4}\frac{dPO_4}{dt} + \frac{\partial pCO_2}{\partial SIL}\frac{dSIL}{dt}$$

.

Each component was estimated by calculating the pCO_2 with the carbonate chemistry equilibrium constants of the model (Follows et al., 2006), using the detrended and deseasonalized variability of the component of interest and setting the values of the remaining parameters to their long-term means (LeQuéré et al., 2003; McKinley et al., 2004, 2006). The sum of each of the components matches reasonably well with the total pCO_2. An attempt to conduct this decomposition using monthly output did not match well with the overall pCO_2 because of the intramonthly variability lost in the monthly averaging. Therefore, daily output was used in the decomposition.

5.2 Regression of pCO_2 Components onto the NAO

Because the variability of each component only includes the variability from the parameter of interest, the overall magnitudes of variability can only be compared if regressed onto a common index of variability. As discussed in the introduction, the main mode of climate variability over the North Atlantic is the North Atlantic Oscillation. This thesis uses the monthly-mean NAO index, operationally defined as the difference between surface pressures of the Azores high-pressure center and the Icelandic low-pressure center. This data is provided from 1950 to the present from the Climate Prediction Center (http://www.cpc.noaa.gov/products/precip/CWlink/pna/nao_index.html). The NAO is moderately correlated with the PC1 of the pCO_2 ($r=0.41$), suggesting that the NAO has a significant relationship to the carbon dynamics in the North Atlantic.

Following the method in McKinley et al. (2006), each component was regressed onto the NAO index for overall comparison. The influences of salinity, phosphate, and silicate on the pCO_2 were found to be marginally significant for overall pCO_2 variability and are therefore excluded from subsequent analysis. Figure 13 shows the regression of pCO_2 and the SST, DIC, and ALK components onto the NAO. The overall pCO_2 regression shows a similar "tripole" pattern traditionally associated with the NAO (Hurrell and Dickson, 2004). Compared to each of the components, the total pCO_2 shows relatively low variability associated with variability in the NAO. Each of the components, however, shows localized centers of high variability influenced by the NAO, but these centers partially cancel each other out in the overall pCO_2. In the subpolar gyre, the NAO seems to drive a significant increase in pCO_2 variability due to

DIC, but this is balanced by a decrease in pCO_2 due to SST. Overall, the variability in total pCO_2 with respect to the NAO is small in the subpolar gyre. Similarly in the eastern subtropics, the variability of the SST component associated with NAO variability is balanced by that of the ALK component. The positive signal from the SST component seems to dominate in the overall pCO_2 regression, but the SST component is partially compensated by the ALK component.

5.3 Regression of pCO_2 Components onto the El Nino Southern Oscillation Index

Another dominant index of global climate variability is El Nino-Southern Oscillation (ENSO). Numerous studies have shown some teleconnection impact of ENSO on the climate over the North Atlantic particularly in the tropical and subtropical regions (Bates, 2001; Gouirand et al., 2007; Huang et al., 1998). Regression of pCO_2 and its major components onto the Multivariate ENSO Index (Wolter and Timlin, 1993, 1998), however, does not produce any patterns with significant amplitudes in this model, aside from some small influences in the equatorial (Figure 14). This suggests that ENSO is only marginally important in the carbon cycle of the North Atlantic. Further analysis in this thesis will focus on the NAO as the main index of climate variability in the North Atlantic.

5.4 Mechanisms driving pCO_2 variability related to the NAO

As discussed in the introduction, the NAO impacts pressure, winds, temperature, and precipitation, all of which impact the surface pCO_2 and CO_2 flux. So, the mechanisms of variability in the NAO may be important drivers on the carbon system. From this

model's results, the two important regions of high pCO_2 component variability are in the subpolar gyre (where pCO_2-SST and pCO_2-DIC dominate the carbon system and balance each other) and in the eastern subtropical gyre (where pCO_2-SST and pCO_2-ALK dominate and balance).

In the subpolar gyre, pCO_2-SST and pCO_2-DIC variability dominate overall pCO_2 variability related to the NAO. As discussed in section 3.2, this is a region where dynamics dominates the carbon system. This mixing is driven by changes in temperature related to the net heat flux. Variability of the net heat flux forcing used in the model is strongly related to NAO variability in this region (Figure 15a). Thus, the mechanism for carbon cycle variability in the subpolar gyre is as follows: (1) changes in the net heat flux of the model are in part driven by changes in the NAO; (2) These changes in the heat flux drive changes in the temperature of the surface waters, which has a direct impact on the pCO_2-SST component of this region; (3) Because this region is dynamics-dominated, the changes in temperature also drive changes in the mixing and surface supply of DIC from depth, which controls the total pCO_2 response. This temperature-driven mixing and supply of DIC is evident in the pCO_2-DIC. Due to the sign in the overall pCO_2 regression matching that of the pCO_2-DIC regression in this subpolar region, the supply of DIC is clearly dominating the overall pCO_2.

The forces driving pCO_2-SST and pCO_2-ALK in the eastern subtropics, however, are a bit more complex because the mechanisms driving these two components are different. Although the signal is not quite as strong as in the subpolar region, pCO_2-SST is still driven by changes in Qnet in the eastern subtropics (Figure 15a), suggesting a similar mechanism driving the pCO_2-SST component as seen in the subpolar gyre.

ALK is not affected by temperature, but freshwater input/removal from changes in evaporation and precipitation related to variability in the NAO can drive ALK variability. To confirm that freshwater variability is indeed the mechanism driving subtropical ALK variability, Figure 15b shows that surface salinity variability also exhibits a similar spatial structure when regressed onto the NAO. Indeed, freshwater climate forcing has a strong impact on the surface ocean in this region. In a study of the ocean precipitation and the NAO using the same NCEP forcings as this model, Mariotti and Arkin (2007) find a significant negative correlation between precipitation and the winter (December, January, February) NAO index in the eastern sub-tropical North Atlantic in a region, spatially coincident with the structures seen in the regressions of model pCO_2-ALK and SSS onto the NAO. Thus, the following mechanism is inferred: increases in the NAO index drive a decrease in precipitation over the ocean; this decrease in surface freshwater input increases ALK, which increases the concentration of HCO_3^- and CO_3^{2-}, decreasing the concentration of $H_2CO_3^*$, causing a decrease in pCO_2.

Because the NAO index is defined as the difference between point-location sea level pressure measurements at the Icelandic Low and the Azores High (Hurrell & Dickson, 2004), it would seem plausible that the locations of high correlation between pCO_2 components and the NAO index would be a function of the location of the NAO measurements (i.e. highest correlations at the Icelandic Low and Azores High measurements). Not surprisingly, those locations closest to the NAO measurement locations should be highly correlated. But does this mean that the relationships discussed above are not physical and only have to do with point location effects? Indeed, regions of high correlation between pCO_2 components and the NAO are nearly spatially

coincident with measurement locations, especially the eastern subtropical gyre region, which is centered nearly on top of the Azores, with correlation tapering off evenly away from the center. There is less prominent a "bull's-eye" in the subpolar region, suggesting that the relationships are more due to regional influences of the NAO on climate forcing than due to point-location effects.

The subtropical "bull's-eye" is more prominent suggesting that point-location effects may be an issue. However, as discussed in section 3.1, this region is also a center of high overall variability for SST and surface ALK (Figures 10b & 10d), the two variables of interest in this region. Thus, while point effects may be an issue, the high variability of this region suggests that the strong signals relating pCO_2-SST and pCO_2-ALK variability to the NAO are robust.

There is some evidence for regional NAO effects on carbon variability, particularly in the subpolar region, but point-location effects in the subtropics suggest that the NAO index is not perfect and does not always explain basin-wide variability. Bakalian et al. (2007) suggest that the Icelandic Low and Azores High are not stationary features, but exhibit considerable north-south displacement. The current convention used to define the NAO index does not include such displacement. As shown in this discussion on the possibility of point-locations effects, the displacement of the index points may be important when considering basin-wide pCO_2 variability.

5.5 Other Modes of Variability and EOF analysis

So far the overall pCO_2 variability has been explained in the subpolar and subtropical regions as a balance between pCO_2 components. A closer look at the regression of the

total pCO_2 onto the NAO yields a local maximum at the interface between the subpolar and subtropical gyres, near the Grand Banks (Figure 13a). On first analysis, this minimum appears to be due to an unbalanced pCO_2-SST component that may be dominating the variability of this region, but as discussed above, the NAO only moderately correlates with the first mode of variability in the model (PC1). Could there be other modes of variability within the model results that account for this structure or other structures more dominant than what is seen with respect to the NAO?

Using PC1 as the main mode of temporal variability in the data, each of the dominant pCO_2 components was regressed onto PC1 (Figure 16). These regressions result in a pattern of variability with different regions of dominance and greater amplitude. The overall magnitude of these regressions is larger than that seen in the NAO regression. Values in the regression onto the PC1 range from below -20 to nearly 20 μatm/1σ PC1 are greater than values in the regression onto the NAO ranging from about -10 to 15 μatm/1σ NAO, suggesting that the PC1 regressions are more robust features.

Similar to the NAO regressions, the total pCO_2 regression shows spatial variability in a tripole pattern with centers of variability in the subpolar region, near the Grand Banks, and in the subtropical region (a fourth center of variability could also be considered south of 15˚N, somewhat seen in the NAO regressions as well). Also like the NAO regressions, the total pCO_2 shows relatively low variability compared to each of the components, such that opposing components show regions of high variability that partially cancel each other out in the overall pCO_2.

The spatial arrangement of pCO_2 component variability is different from that seen in the NAO regressions, particularly in the subpolar gyre where there is little to no signal of balancing variability between pCO_2-DIC and pCO_2-SST. Most variability in the components is confined to the subtropical gyre south of 50˚N. However, because the EOF is finding the first mode of area-weighted variability, the variability in the subtropical gyre should stand out due to the larger area of grid cells at lower latitudes. Similarly, the NAO should have a larger impact on subpolar components because of the index's definition (discussed above). The correlation between the NAO index and PC1 is only 0.41, and these subpolar distinctions may drive much of the difference in the indices.

Overall pCO_2 variability is mostly dominated by the pCO_2-SST component, with high variability in the eastern subtropical gyre and along the eastern U.S. The pCO_2-SST component is strongly balanced by the pCO_2-DIC component with a spatial pattern similar to that of the pCO_2-SST. The eastern subtropical variability maximum in the pCO_2-SST is also balanced by a local maximum in pCO_2-ALK, similar to the pattern in the NAO regression, suggesting that a freshwater forcing is a robust signal in the overall climate forcing and carbon cycle response at this location.

One location where total pCO_2 variability is not dominated by the pCO_2-SST component is near the Grand Banks (location centered at 45˚N, 30˚W). Here, pCO_2-SST variability is insignificant, but pCO_2-DIC variability is moderately strong, dominating the overall pCO_2 variability. This region, however, is located right at the interface between the temperature-dominant and dynamics-dominant regions, such that neither temperature nor mixing changes can serve as a mechanism to explain the pCO_2 variability of this

region. The shape of the pCO_2-DIC regression does seem to indicate some amount of horizontal advection of DIC following the location of the Gulf Stream with high values of pCO_2-DIC along the eastern U.S. slowly decreasing to the northeast. Similar to the model parameter of DIC vertical supply discussed in section 3.3, the model is also able to output the horizontal supply of DIC as the size of the flux of DIC between lateral grid cells. Regression of this term onto the PC1 (Figure 17) shows that the DIC horizontal supply in this region is strongly related to changes in the PC1. Clearly changes in the pCO_2 related to the PC1 near the Grand Banks are driven by variability in the horizontal supply of DIC to this region. In addition, changes in pCO_2 and DIC concentrations in the top 100m are strongly correlated with the horizontal supply at this region of interest (Figure 18), further suggesting that variability in horizontal transport drives much of the carbon dynamics of this region.

Despite issues discussed in section 2.7 about introduced trends in the data related to a lack of horizontal transport from the south, this horizontal supply of DIC to the Grand Banks does relate well to recent research and observational reports. The increasing trend in the detrended pCO_2 PC1 from 1995-2006 (Figure 9c) means that the patterns seen in the regression plots have intensified during this period, suggesting that the horizontal supply of DIC to the Grand Banks has increased. Hatun et al. (2005) show that subpolar gyre deceleration is accompanied by stronger advection of subtropical waters by North Atlantic Current extension. Autonomous glider data (Hakkinen & Rhines, 2007) have verified this increase in advection of subtropical waters. The trend in the PC1 also seems to match the decrease in sea-surface-height-derived geostrophic velocity (satellite data) in the subpolar gyre since 1994 (Hakkinen & Rhines, 2004).

Therefore, the model results support the notion of an increase in DIC horizontal supply to the Grand Banks region, potentially from the stronger advection of subtropical waters, due to a weakening of the subpolar gyre.

Assuming that this trend in the North Atlantic is real (as verified by this thesis and other sources), it is important in understanding the carbon system as such changes in horizontal advection of DIC may confound other carbon findings in the North Atlantic. For instance, Schuster & Watson (2007) report on volunteer ship track data between the Caribbean and the U.K. (a useful dataset that spans the regions of interest with respect to increased horizontal supply of DIC). They report on a decreased sink of atmospheric CO_2 through an increase of 21 μatm in surface pCO_2 from 1994/95 to 2002/2005. Certainly there has been an increase in atmospheric CO_2 during this time period, and such an increase will drive more CO_2 into the surface ocean, limited by the buffering capacity of seawater (i.e. the Revelle Factor). The results of this thesis, however, show that some of this regional increase in surface pCO_2 may be attributable to enhanced horizontal transport of DIC from the subtropics. This example is highlighted to stress that the ocean carbon cycle is a four dimensional entity (time included) and that limiting this view to two dimensions may be drastically oversimplifying the system, such that important shifts in the dynamical transport may be improperly neglected.

6. SUMMARY AND CONCLUSIONS

6.1 Summary

The main goal of this thesis was to develop a better understanding of the mechanisms that drive carbon cycle variability in the North Atlantic. Results show that high interannual

variability in pCO_2, SST, DIC, and ALK is mainly confined to the subtropics. This is a region where temperature effects dominate pCO_2 variability. Subpolar gyre pCO_2, however, is dominated by variability related to dynamics, where changes in temperature control the deep mixing and upwelling of DIC.

Overall pCO_2 variability is constrained through opposing effects related to SST, DIC, and ALK. Such a "balancing act" of pCO_2 components and their variability has been shown here in regression onto the NAO index and the PC1 of the pCO_2. SST is important in subtropical waters where the pCO_2 variability is "temperature-dominated." SST is also important in subpolar NAO-driven pCO_2 variability in that it is a major driver for mixing variability in this region. DIC impacts on pCO_2 variability are also seen throughout much of the basin, with strong DIC variability related to horizontal advection in the subtropics and mixing in the subpolar gyre. ALK impacts on pCO_2 variability seem to be confined to the eastern subtropical gyre, where freshwater/evaporation influences are particularly strong. The influences of ALK variability on overall pCO_2 are balanced by SST variability in this region.

6.2 Total Basin CO_2 Flux Variability

The results of this thesis have focused on regional mechanisms driving carbon cycle variability, but how does all this fit together in potential impacts on the global flux variability? As discussed in section 1.2, one of the debates in North Atlantic carbon cycle research relates to estimating the total basin-wide flux variability. The basin wide CO_2 flux interannual variability magnitude was calculated by finding the root mean

squared (RMS) of the area-weighted sum of the detrended and smoothed (12-month) flux field. RMS results for various bands of latitude range are displayed in Table 2.

Table 2: Basin wide area-weighted sum of CO_2 flux interannual variability RMS.

LOCATION	LATITUDE RANGE	RMS (Pg C yr^{-1})
Subpolar	50N – 80N	0.01
Subtropical	14N – 50N	0.03
Tropical	-14N – 14N	0.02
Subpolar + Subtropical	14N – 80N	0.03
Total North Atlantic	-14N – 80N	0.05

These results are in line with previous forward model estimates (McKinley et al., 2004; Obata and Kitamura, 2003; Le Quéré et al., 2000). The total North Atlantic variability is small relative to global flux variability, suggesting that the North Atlantic does not play a substantial role on the global flux variability. These findings further contradict the extrapolation estimates of Gruber et al. (2002) and inverse modeling results (Bousquet et al., 2000) that put the North Atlantic flux variability near ±0.3 Pg C yr^{-1}. Much work was put into the setup of the model used in this thesis to maximize variability (turning off relaxation terms), yet overall flux variability is still an order of magnitude smaller than extrapolated and inverse modeled estimates. While this model does not capture the physical variability due to mesoscale eddies and boundary conditions, the flux variability found in this thesis and in other forward model results in the North Atlantic suggests that it is insignificant in the global flux variability.

6.3 Future Work

This thesis has produced some interesting results with regard to the carbon cycle mechanisms in the North Atlantic and their response to climate variability, but the work is not done. As discussed in the introduction, these results are limited by a lack of heat flux convergence into the western subtropics, resulting in a climate-forced cooling trend not manifested in observations due to reduced simulated southerly flow supplying warm water to this region. Future work with this model should look to improve the temperature discrepancies by finding ways to enhance the transport and modify the temperature relaxation techniques.

One idea to improve the circulation along the southern boundary would be to create an open boundary (the run in this thesis used a closed southern boundary with sponge layer), using velocity fields from output of another high-resolution general circulation model not limited to the North Atlantic. One possibility would be to use output from the Estimating the Circulation & Climate of the Ocean (ECCO) Project. ECCO combines a general circulation model (the same model as used in this thesis) with observational and remote sensing data to produce a high-resolution representation of the ocean state through time (http://www.ecco-group.org/). Velocity fields along the southern boundary can be forced by ECCO output in hopes of producing a circulation state that is more like reality.

The other way to improve the issues with subtropical SSTs will be to find ways to enhance the heat forcing and relaxation directly. The ECCO project also provides adjusted net heat flux fields that incorporate ocean observational data. Preliminary results using this data show that there is less of a subtropical SST cooling trend from the

early 1990's to the 2000's (via correspondence with Dr. Stephanie Dutkiewicz at MIT). This seems to suggest that the NCEP heat flux forcing used in this thesis may not be entirely correct, and the use of ECCO heat flux forcings may be a step in the right direction.

Another opportunity for improvement in the model may come in finding ways to modify the relaxation techniques. Indeed, T and S relaxation is necessary for model stability, but it removes much of the interannual variability in the model. A limitation in the model setup of this thesis is that T and S were relaxed to climatological values. WOA climatology is certainly the only data available for the ocean basin, but perhaps satellite SST data can be assimilated to create time-varying relaxation fields (at least for the surface layer). This may limit the variability that is lost through relaxation to climatology.

All of this work supports the need for more observational data to constrain ocean carbon models. Certainly, the timeseries data available from BATS has been invaluable in this thesis for model validation and understanding limitations in the results. Much this work has shown that BATS is an apt location for studying carbon cycle variability in the North Atlantic, as it is situated in a region of high pCO_2 variability (Figure 10a), such that understanding the long term trends at BATS may help to better understand basin-wide subtropical variability. Another useful timeseries is the ESTOC station (European Time Series in the Canary Islands) (Santana-Casiano et al., 2003, 2007). As shown in this thesis, the eastern subtropical gyre is a region of high ALK- and T-driven pCO_2 variability, and ESTOC is conveniently situated near this center of action. Data from this

timeseries was unavailable for use in this thesis, but the importance of this region in understanding pCO_2-component variability may spur future collaboration.

REFERENCES

Anderson, L.A. and J.L. Sarmiento (1994), Redfield ratios of remineralization determined by nutrient data analysis. *Global Biogeochem. Cycles*, 8(1), 65–80.

Antonov, J. I., R. A. Locarnini, T. P. Boyer, A. V. Mishonov, and H. E. Garcia (2006), *World Ocean Atlas 2005, Volume 2: Salinity,* S. Levitus, Ed., NOAA Atlas NESDIS 62, U.S. Government Printing Office, Washington, D.C., 182 pp.

Bakalian F., S. Hameed, R. Pickart (2007), Influence of the Icelandic Low latitude on the frequency of Greenland tip jet events: Implications for Irminger Sea convection, *J. Geophys. Res.*, 112, C04020, doi:10.1029/2006JC003807.

Bates, N.R. (2001), Interannual variability of oceanic CO_2 and biogeochemical properties in the Western North Atlantic subtropical gyre, *Deep-Sea Research II*, 48, 1507-1528.

Bates, N.R. (2007), Interannual variability of the oceanic CO_2 sink in the subtropical gyre of the North Atlantic Ocean over the last 2 decades, *J. Geophys. Res.*, 112, C09013, doi:10.1029/2006JC003759.

Bennington, V., G.A. McKinley, S. Dutkiewicz, D.J. Ullman, (in prep.), What interannual Chl variability tells us about North Atlantic CO_2 flux variability.

Bersch, M. (2002), North Atlantic Oscillation-induced changes of the upper-layer circulation in the northern North Atlantic Ocean, *J. Geophys. Res*., 107(C10), 3156, doi: 10.1029/2001JC000901.

Bethoux, J.P., P. Morin, C. Chaumery, O. Connan, B. Gentili, and D. Ruiz-Pino (1998), Nutrients in the Mediterranean Sea, mass balance and statistical analysis of concentrations with respect to environmental change, *Marine Chemistry*, 63, 155–169.

Bojariu, R., and G. Reverdin, (2002), Large-scale variability modes of freshwater flux and precipitation over the Atlantic, *Climate Dynamics*, 18(5), 369-381.

Bousquet, P, P. Peylin, P. Ciais, C. Le Quéré, P. Friedlingstein, and P. Tans (2000), Regional changes in carbon dioxide fluxes of land and oceans since 1980. *Science*, 290(5495), 1342.

Conway, T. J., P.P. Tans, L.S. Watermann, K.W. Thoning, D.R. Kitzis, K.A. Masarie, and N. Zhang (1994), Evidence for interannual variability of the carbon cycle from the National Oceanic and Atmospheric Administration/Climate Monitoring and Diagnostics Laboratory Global Air Sampling Network, *J. Geophys. Res*., 99(D11), 22,831–22,855.

Cunningham, S.A., T. Kanzow, D. Rayner, M.O. Baringer, W.E. Johns, J. Marotzke, H.R. Longworth, E.M. Grant, J.J.-M. Hirschi, L.M. Beal, C.S. Meinen, and H.L. Bryden

(2007), Temporal Variability of the Atlantic Meridional Overturning Circulation at 26.5°N, *Science,* 317, 935-938.

Dutkiewicz, S., M. J. Follows, and P. Parekh (2005), Interactions of the iron and phosphorus cycles: A three-dimensional model study, *Global Biogeochem. Cycles*, 19, GB1021, doi:10.1029/2004GB002342.

Follows, M.J., S. Dutkiewicz, and T. Ito (2006), On the solution of the carbonate system in ocean biogeochemistry models, *Ocean Modeling*, 12, 290-301.

Gent, P. R., and J. C. McWilliams (1990), Isopycnal mixing in ocean general circulation models, *J. Phys. Oceanogr*., 20, 150–155.

Gouirand, I., V. Moron, and E. Zorita (2007), Teleconnections between ENSO and North Atlantic in an ECHO-G simulation of the 1000-1990 period, *Geophysical Research Letters*, 34, L06705, doi:10.1029/2006GL028852.

Gruber, N., C. D. Keeling, and N. R. Bates (2002), Interannual variability in the North Atlantic Ocean carbon sink, *Science*, 298, 2374–2378.

Gurney, K., et al. (2002), Towards robust regional estimates of CO_2 sources and sinks using atmospheric transport models, *Nature*, 415, 626–630.

Häkkinen, S. and P.B. Rhines (2004), Decline of Subpolar North Atlantic Circulation During the 1990s, *Science*, 304, 555-559.

Hakkinen, S. and P.B. Rhines, (2007) Shifting surface currents in the northern North Atlantic Ocean*, J. Marine Res*., submitted.

Hátún, H., B. Hansen, A. B. Sandø, H. Drange, and H. Valdimarsson (2005), De-stabilization of the North Atlantic Thermohaline Circulation by a Gyre Mode, *Science*, 309, 1841-1844.

Huang, J., K. Higuchi, and K. L. Shabbar (1998), The relationships between the North Atlantic Oscillation and El Niño Southern Oscillation, *Geophys. Res. Lett*., 25, 2707-2710.

Hurrell, J.W., and R.R. Dickson (2004), *Climate variability over the North Atlantic. Marine Ecosystems and Climate Variation - the North Atlantic*, N.C. Stenseth, G. Ottersen, J.W. Hurrell, and A. Belgrano, Eds. Oxford University Press, 15-31.

Hurrell, J. W., Y. Kushnir, G. Ottersen, and M. Visbeck (2003), An overview of the North Atlantic Oscillation. The North Atlantic Oscillation: Climatic Significance and Environmental Impact. J. W. Hurrell, Y. Kushnir, G. Ottersen, and M. Visbeck, Eds. *Geophysical Monograph*, 134, 1-35.

Kalnay, E., et al. (1996), The NCEP/NCAR 40-Year Reanalysis Project, *Bull. Am. Meteorol. Soc*., 77, 437–471.

Keeling, R. F., S. C. Piper, and M. Heimann (1996), Global and hemispheric CO_2 sinks deduced from changes in atmospheric O2 concentration, *Nature*, 381, 150–155.

Keeling, C.D. and T.P. Whorf (2005), Atmospheric CO_2 records from sites in the SIO air sampling network. In Trends: A Compendium of Data on Global Change. Carbon Dioxide Information Analysis Center, Oak Ridge National Laboratory, U.S. Department of Energy, Oak Ridge, Tenn., U.S.A.

Kilpatrick, K.A., G.P. Podesta and R. Evans (2001), Overview of the NOAA/NASA Advanced Very High Resolution Radiometer Pathfinder algorithm for sea surface temperature and associated matchup database, *J. Geophys. Res.-Oceans*, 106 (C5), 9179-9197.

Large, W.G., J.C. McWilliams, and S.C. Doney (1994), Oceanic vertical mixing: A review and a model with a nonlocal boundary layer parameterization, *Rev. Geophys*., 32, 363–403.

Le Quéré , C., J.C. Orr, P. Monfray, O. Aumont, and G. Madec (2000), Interannual variability of the oceanic sink of CO_2 from 1979 to 1997*, Global Biogeochem. Cycles*, 14, 1247–1265.

LeQuéré , C., O. Aumont, P. Monfray, and J.C. Orr (2003), Propagation of climatic events on ocean stratification, marine biology, and CO_2: Case studies over the 1979 – 1999 period, *J. Geophys. Res*., 108(C12), 3375, doi:10.1029/2001JC000920.

Locarnini, R.A., A.V. Mishonov, J.I. Antonov, T.P. Boyer, and H.E. Garcia (2006), *World Ocean Atlas 2005, Volume 1: Temperature*, S. Levitus, Ed., NOAA Atlas NESDIS 61, U.S. Government Printing Office, Washington, D.C., 182 pp.

Luo, C., N. Mahowald, and J. del Corral (2003), Sensitivity study of meteorological parameters on mineral aerosol mobilization, transport and distribution, *J. Geophys. Res*., 108 (D15), 4447.

Mahowald, N., C. Luo, J. del Corral, and C. Zender (2003), Interannual variability in atmospheric mineral aerosols from a 22-year model simulation and observational data, *J. Geophys. Res*, 108 (D12).

Mann, K.H., and J.R.N. Lazier (1996), *Dynamics of marine ecosystems. Biological-physical in interactions in the oceans*, 2nd Edn. Blackwell Science, Massachusetts, U.S.A., 394 pp.

Mariotti, A. and P. Arkin (2007), The North Atlantic Oscillation and oceanic precipitation variability, *Climate Dynamics*, 28, 35-51.

Marshall, J.C., C. Hill, L. Perelman, and A. Adcroft (1997a), Hydrostatic, quasi-hydrostatic and non-hydrostatic ocean modeling, *J. of Geophys. Res.*, 102, 5733–5752.

Marshall, J. C., A. Adcroft, C. Hill, L. Perelman, and C. Heisey (1997b), A finite volume, incompressible Navier-Stokes model for studies of the ocean on parallel computers, Journal of Geophysical Research, 102, 5753–5766.

Marshall, J., Johnson, H. and J. Goodman (2001), Interaction of the North Atlantic Oscillation with ocean circulation, *Journal of Climate*, 14(7), 1399-1421.

McKinley, G.A., M.J. Follows and J.C. Marshall (2000), Interannual variability of the air-sea flux of oxygen in the North Atlantic, *Geophys. Res. Lett.*, 27(18), 2933-2936, 2000.

McKinley, G. A., M. J. Follows, and J. Marshall (2004), Mechanisms of air-sea CO_2 flux variability in the equatorial Pacific and the North Atlantic, *Global Biogeochem. Cycles*, 18, GB2011, doi:10.1029/2003GB002179.

McKinley, G.A., T. Takahashi, E. Buitenhuis, F. Chai, J. R. Christian, S. C. Doney, M.-S. Jiang, C. Le Quere, I. Lima, K. Linday, J.K. Moore, R. Murtugudde, L. Shi, and P.Wetzel (2006), North Pacific carbon cycle response to climate variability on seasonal to decadal timescales. *J. Geophys Res*., 111, C07S06, doi:10.1029/2005JC003173.

Mignot, J., and C. Frankignoul (2003), On the interannual variability of surface salinity in the Atlantic, *Climate Dynamics*, 20(6), 555–565

Monterey, G., and S. Levitus (1997), Seasonal Variability of Mixed Layer Depth for the World Ocean, NOAA Atlas, NESDIS 14, *Natl. Oceanic and Atmos. Admin*., Silver Spring, Md., 100 pp.

Obata, A., and Y. Kitamura (2003), Interannual variability of the sea-air exchange of CO_2 from 1961 to 1998 simulated with a global ocean circulation-biogeochemistry model. *J. Geophys. Res.*, 108 (C11), 3337.

Omar, A.M., T. Johannessen, A. Olsen, S. Kaltin, and F. Rey (2007), Seasonal and interannual variability of the air-sea CO_2 flux in the Atlantic sector of the Barents Sea, *Marine Chemistry,* 104(3-4), 203-213.

Parekh, P., M.J. Follows, and E.A. Boyle (2004), Modeling the global ocean iron cycle, *Global Biogeochem. Cycles*, 18, GB1002, doi:10.1029/2003GB002061.

Peylin, P., P. Bousquet, C. Le Quéré, S. Sitch, P. Friedlingstein, G. McKinley, N. Gruber, P. Rayner, and P. Ciais (2005), Multiple constraints on regional CO_2 flux variations over land and oceans, *Global Biogeochem. Cycles*, 19, GB1011, doi:10.1029/2003GB002214.

Reynolds, R.W. and T.M. Smith (1994), Improved global sea surface temperature analyses using optimum interpolation. *J. Climate*, 7, 929-948.

Sabine, C.L. , R.A. Feely, N. Gruber, R.M. Key, K. Lee, J.L. Bullister, R. Wanninkhof, C.S. Wong, D.W.R. Wallace, B. Tilbrook, F.J. Millero, T-H Peng, A. Kozyr, T. Ono, and A.F. Rios (2004), The oceanic sink for anthropogenic CO_2, *Science*, 305(5682), 367-371.

González-Dávila, M., J.M. Santana-Casiano, M.J. Rueda, O. Llinás, and E.F. González-Dávila (2003), Seasonal and interannual variability of sea-surface carbon dioxide species at the European Station for Time Series in the Ocean at the Canary Islands (ESTOC) between 1996 and 2000, *Global Biogeochem. Cycles,* 17(3), 1076 doi:10.1029/2002GB001993.

Santana-Casiano, J.M., M. González-Dávila, M.J. Rueda, O. Llinás, and E.F. González-Dávila (2007), The interannual variability of oceanic CO_2 parameters in the northeast Atlantic subtropical gyre at the ESTOC site, *Global Biogeochem. Cycles,* 21, GB1015, doi:10.1029/2006GB002788.

Sarmiento, J.L., and N. Gruber (2002), Sinks for anthropogenic carbon, *Physics Today*, August 2002, 30-36.

Sarmiento, J.L. and N. Gruber (2006), *Ocean Biogeochemical Dynamics*, Princeton University Press, 503 pp.

Schuster, U., and A.J. Watson (2007), A variable and decreasing sink for atmospheric CO_2 in the North Atlantic, *J. Geophys. Res.*, 112 (C11), C11006, doi:10.1029/2006JC003941.

Takahashi, T., J. Olafsson, J.G. Goddard, D.W. Chipman, and S. Sutherland (1993), Seasonal variation of CO_2 and nutrients in the high-latitude surface oceans: A comparative study, *Global Biogeochem. Cycles*, 7(4), 843–878.

Takahashi, T., et al. (2002), Global sea-air CO_2 flux based on climatological surface ocean pCO_2, and seasonal biological and temperature effects, *Deep Sea Res., Part II*, 49, 1601–1622.

Tomczak, M. and J.S. Godfrey (1994), Regional Oceanography: an Introduction Pergamon, Oxford, 442 pp.

Visbeck, M.H., J.W. Hurrell, L. Polvani, and H.M. Cullen (2001). The North Atlantic Oscillation: Past, present, and future. *Proceedings of the National Academy of Sciences*, 98(23).

Wanninkhof , R. (1992), Relationship between wind speed and gas exchange over the ocean, *J. Geophys. Res*., 97, 7373–7382.

Wolter, K., and M.S. Timlin (1993), Monitoring ENSO in COADS with a seasonally adjusted principal component index, Proc. of the 17th Climate Diagnostics Workshop, Norman, OK, NOAA/N MC/CAC, NSSL, *Oklahoma Clim. Survey*, CIMMS and the School of Meteor., Univ. of Oklahoma, 52-57.

Wolter, K., and M.S. Timlin (1998), Measuring the strength of ENSO events - how does 1997/98 rank?, *Weather*, 53, 315-324.

Worthington, L., On the North Atlantic circulation, *Johns Hopkins Oceanographic Studies*, 6, 110, 1976.

Zhang, R., T.L. Delworth, and I.M. Held (2007), Can the Atlantic Ocean drive the observed multidecadal variability in Northern Hemisphere mean temperature?, *Geophys. Res. Lett.*, 34, L02709, doi:10.1029/2006GL028683.

FIGURES

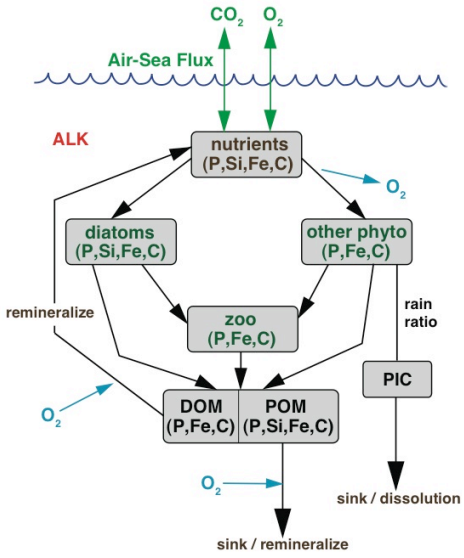

Figure 1. Schematic of ecosystem model from Dutkiewicz et al. (2005) showing the cycling of nutrients (Fe, P, Si) within two classes of phytoplankton, one class of zooplankton, and the two pools of dissolved organic matter (DOM) and particulate organic matter (POM). The model includes both nutrient (P, Fe, Si) and carbon cycling.

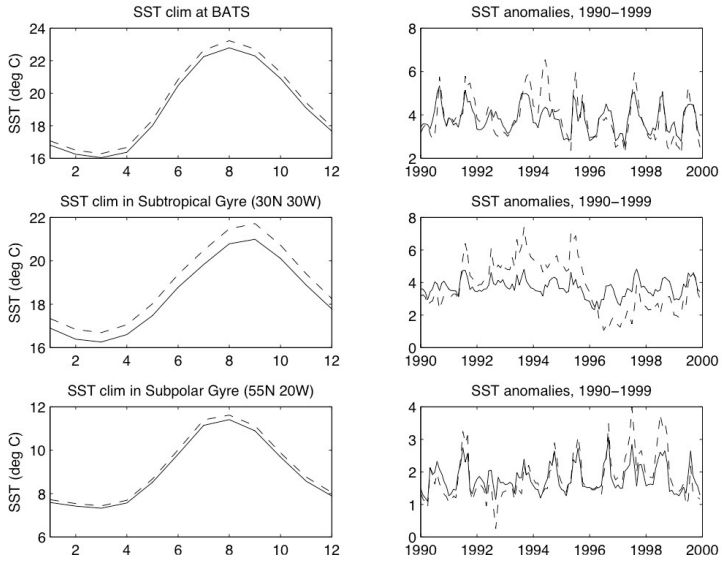

Figure 2. Comparison of SST climatology and SST anomalies (relative to climatology) for a ten-year test run with active relaxation back to observations turned on (solid line) and climatological relaxation terms incorporated into the forcing (dashed line). At 3 separate locations: Bermuda (BATS), Eastern Subtropical Gyre, and Subpolar Gyre. Plots show a minor difference in climatology, but considerable increase in variability as seen from the anomalies.

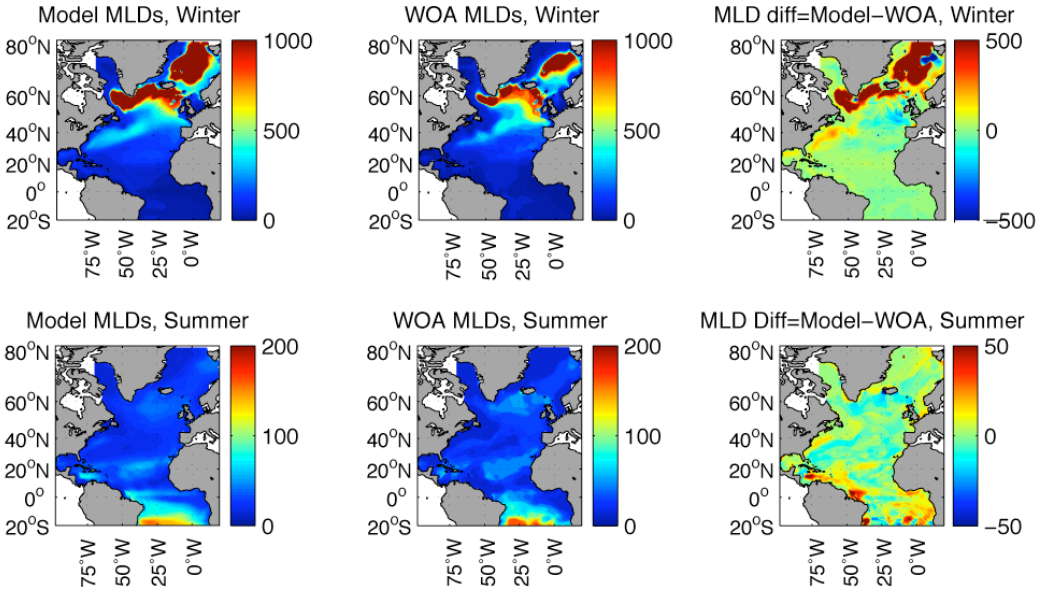

Figure 3. Comparison of seasonal mixed-layer depths for model output and WOA climatology. Winter season constitutes the mean of values in December, January, and February. Summer season constitutes the mean of July, August, and September. The two plots on the far right show the difference between the model output and the observations. Due to deeper MLDs in the winter, please note the difference in colorbar limits.

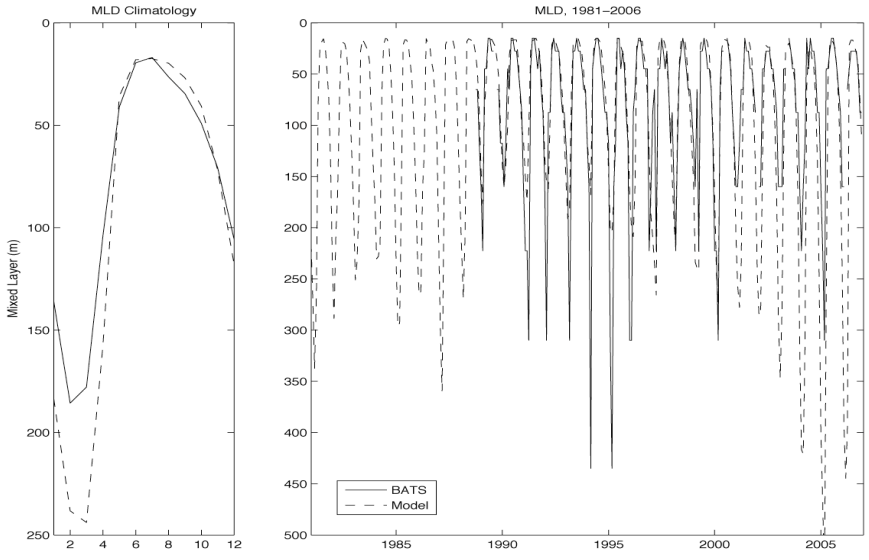

Figure 4. Observed (solid line) and Modeled (dashed line) mixed layer depths at BATS. The left plot shows the mean seasonal cycle and the right plot shows the variability for 1981-2006.

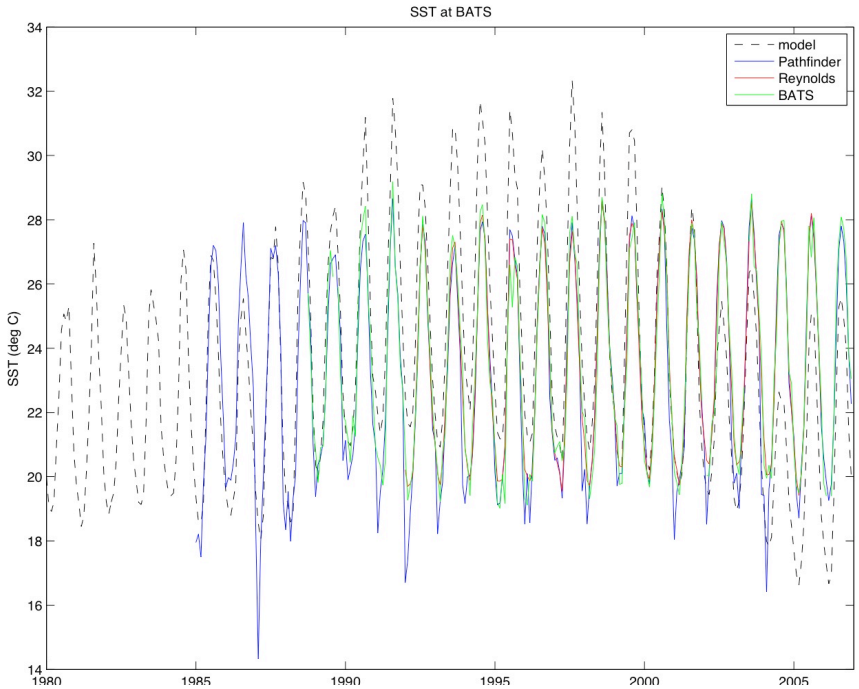

Figure 5. SST from satellite observations (Pathfinder and Reynolds), in situ measurements (BATS), and model output. There is good agreement among satellite estimates and in situ measurements but significant discrepancy between model and data.

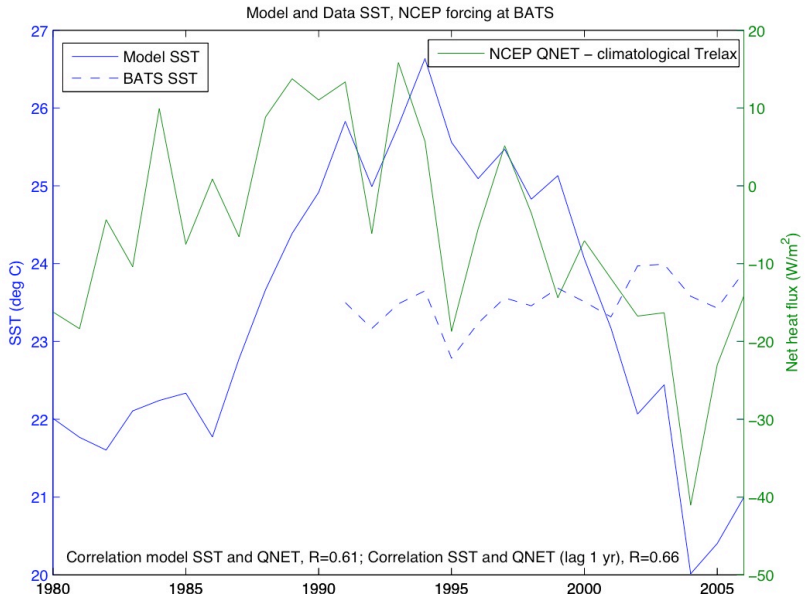

Figure 6. Model and data SST plotted on left axis, net heat flux on right axis. High correlation between model SST and Qnet forcing shows that model is impacted more by net heating than what is seen in the observations.

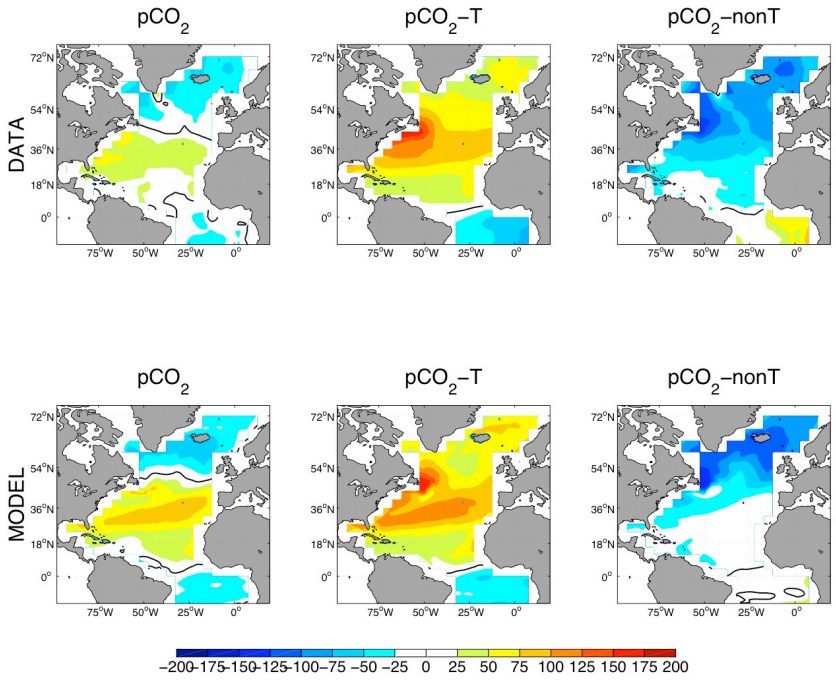

Figure 7. Seasonal cycle of pCO_2 and its temperature and non-temperature components for observed climatological data (Takahashi, 2002) and model output. Calculated by subtracting the mean winter (FMA) pCO_2 values from the mean summer (ASO) values (seasonal average uses 3-month mean). Positive values indicate regions where summer pCO_2 exceeds winter pCO_2. (From Bennington et al., in prep.)

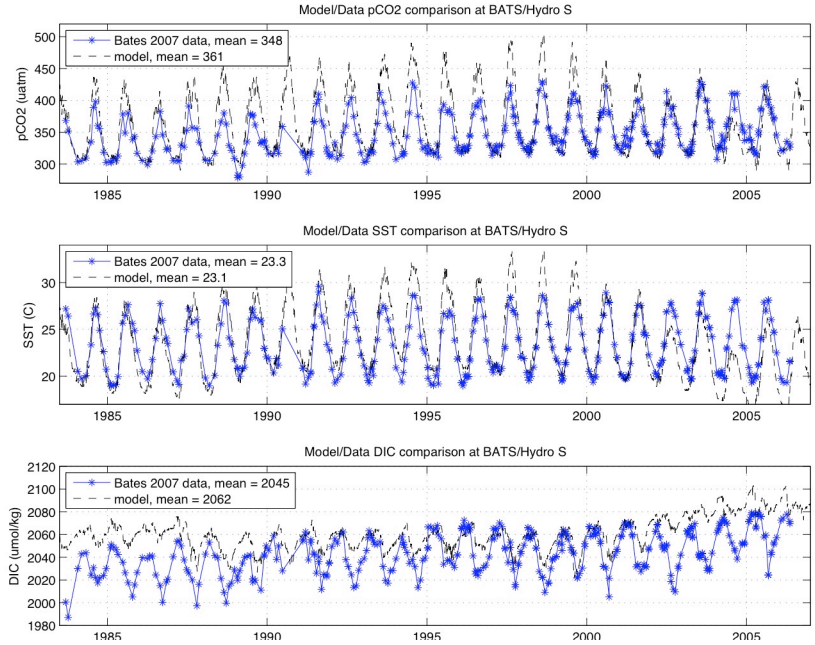

Figure 8. Comparison of (a) pCO_2, (b) SST, and (b) DIC between model results and observations at the Bermuda Atlantic Time-series Study (BATS)/Hydrostation S from 1983 through 2006 (Bates, 2007).

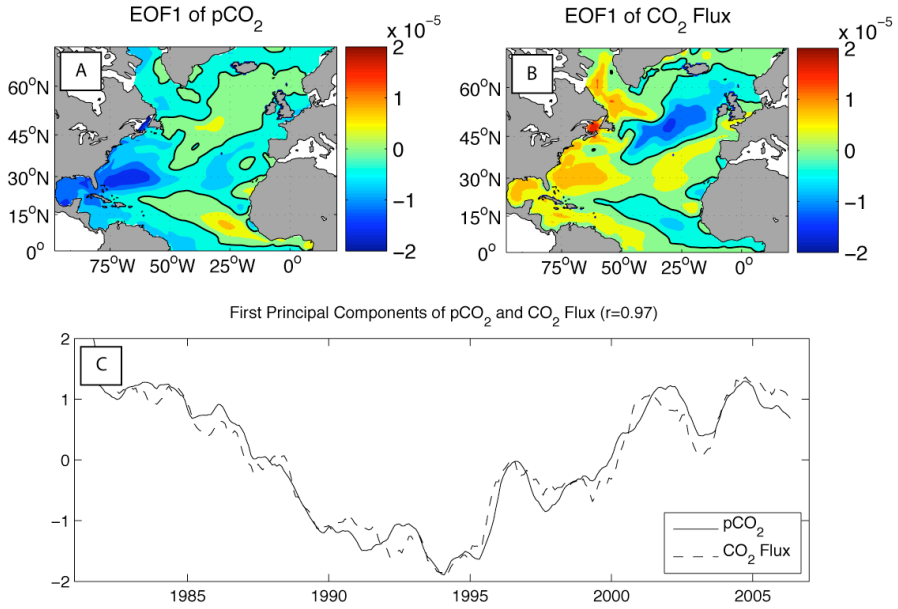

Figure 9. EOF Analysis of detrended pCO_2 and CO2 flux smoothed over 12 months, calculated using output from 1981-2006. (a) First EOF of pCO_2 (explaining 32% overall variance). (b) First EOF of CO_2 Flux (explaining 26% overall variance). (c) First standardized PCs corresponding to EOFs. The two PC1s are highly correlated (r=0.97), suggesting that nearly all the variability in the air-sea flux of CO_2 is driven by the surface pCO_2.

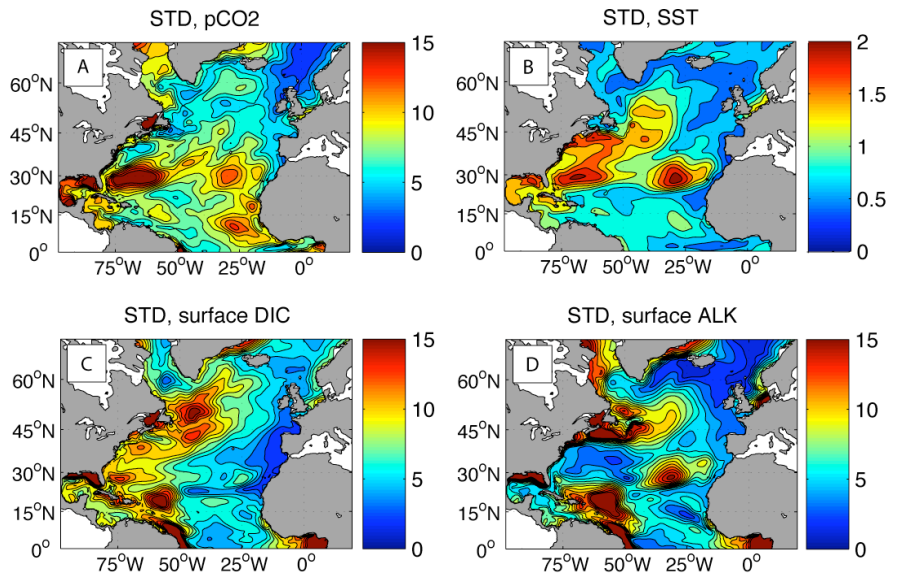

Figure 10. Standard deviation of: (a) pCO_2 (µatm), (b) SST (degrees C), (c) surface DIC (mmol/m^3), and (d) surface ALK (mmol/m^3). All standard deviations were calculated from model output that was detrended and smoothed over 12 months to remove the seasonal cycle.

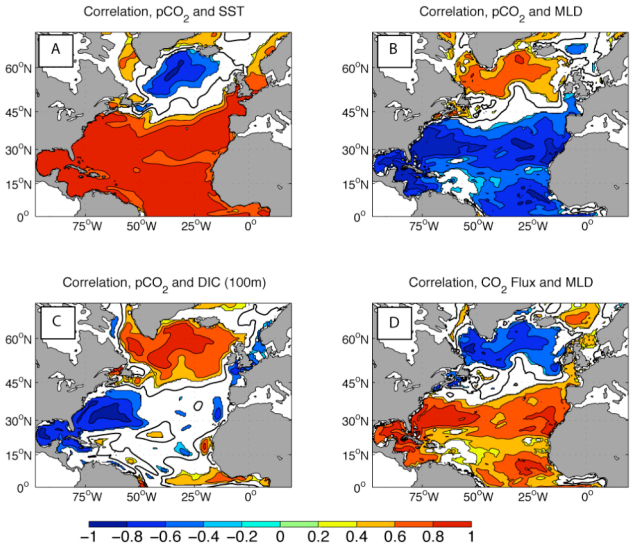

Figure 11. Correlation plots. (a) pCO_2 and SST, (b) pCO_2 and MLD, (c) pCO_2 and 100m depth-weighted DIC, (d) CO_2 Flux (positive to the atmosphere) and MLD. Correlation coefficients were calculated from fields that were detrended and smoothed over 12 months to remove the seasonal cycle. White areas indicate those regions where the correlation coefficient is not significantly different from zero at the 95% level.

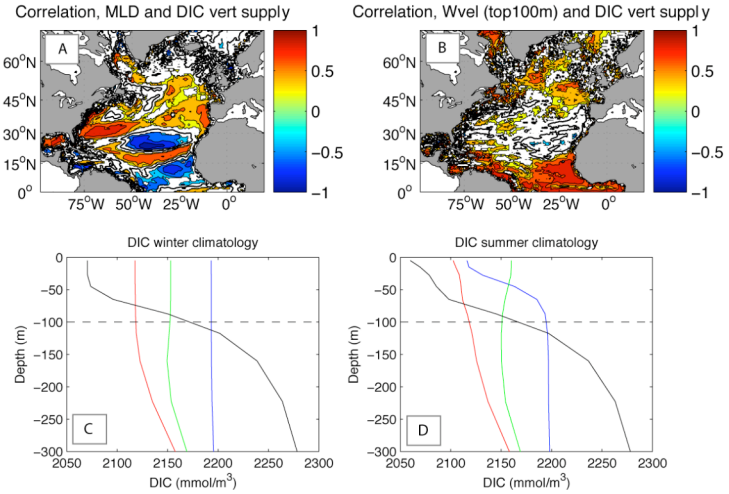

Figure 12. (a) Correlation between MLD and vertical supply of DIC over the top 100m. (b) Correlation between vertical velocity averaged over the top 100m and the DIC vertical supply (top 100m). (c) Depth profiles of DIC concentrations over the top 300m, winter climatology averaged over all January, February, and March months. 4 profiles are for the following locations: BATS, 32N 64W (red); Ocean Weather Station I, 59N 18W (blue); Eastern Subtropical gyre, 25N 40W (green); Southern Subtropical gyre, 10N 30W (black). (d) Depth profiles of late summer climatology averaged over July, August, and September (profile colors pertain to the same locations as in plot c).

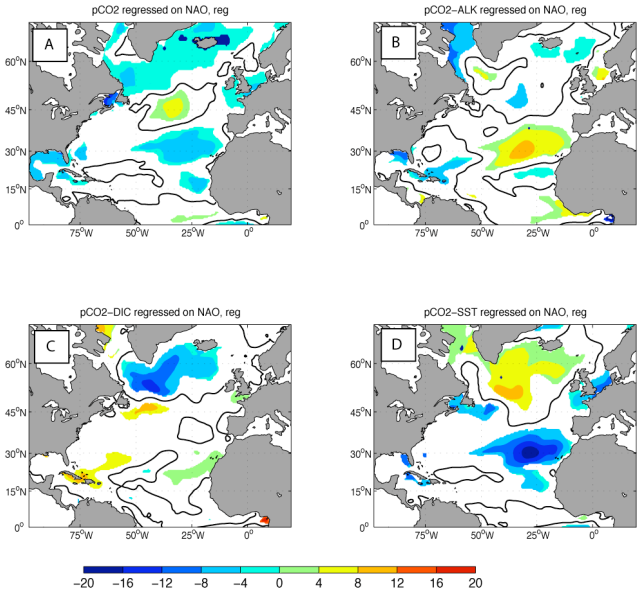

Figure 13. Regression of (a) total pCO_2, (b) pCO_2-ALK, (c) pCO_2-DIC, and (d) pCO_2-SST onto the negative NAO index (negative so that patterns are of the same sign as Figure 16). Units are µatm per 1 standard deviation of the NAO. pCO_2 fields and components are detrended and smoothed. Colored areas indicate regions were the correlation coefficient is significantly different from zero at the 95% confidence level.

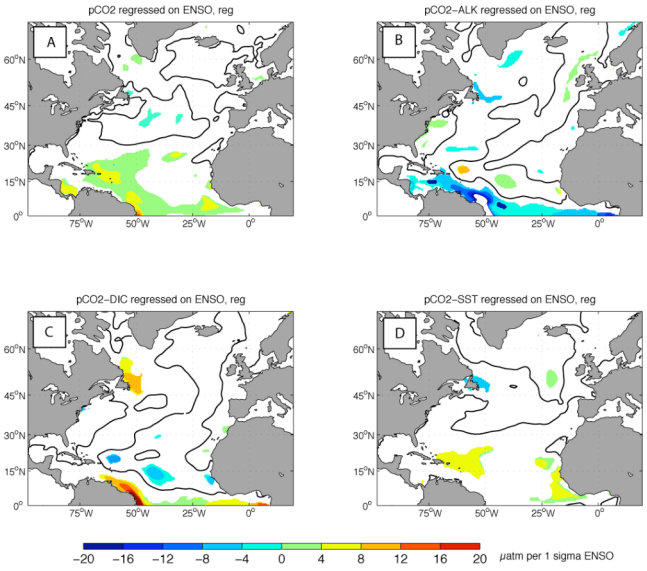

Figure 14. Regression of (a) total pCO_2, (b) pCO_2-ALK, (c) pCO_2-DIC, and (d) pCO_2-SST onto the ENSO. Units are µatm per 1 standard deviation of the ENSO. Colored areas indicate regions were the correlation coefficient is significantly different from zero at the 95% confidence level.

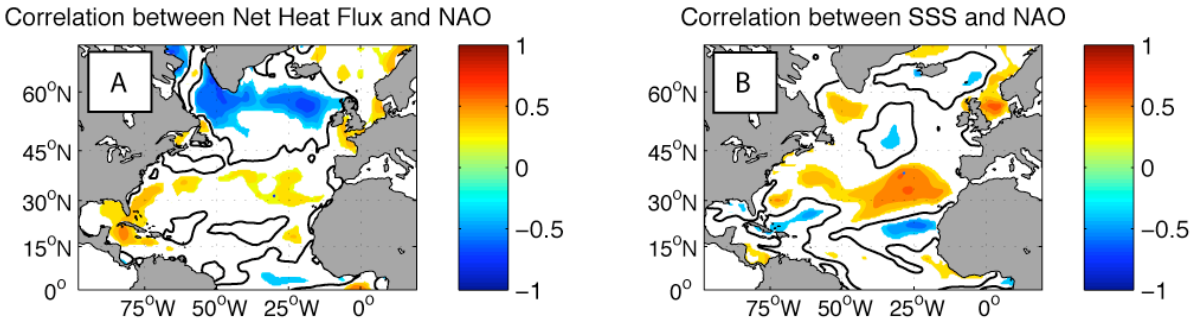

Figure 15. Correlation between the NAO index and (a) Model net heat flux forcing (b) Sea Surface Salinity (detrended and smoothed). Colored areas indicate regions were the correlation coefficient is significantly different from zero at the 95% confidence level.

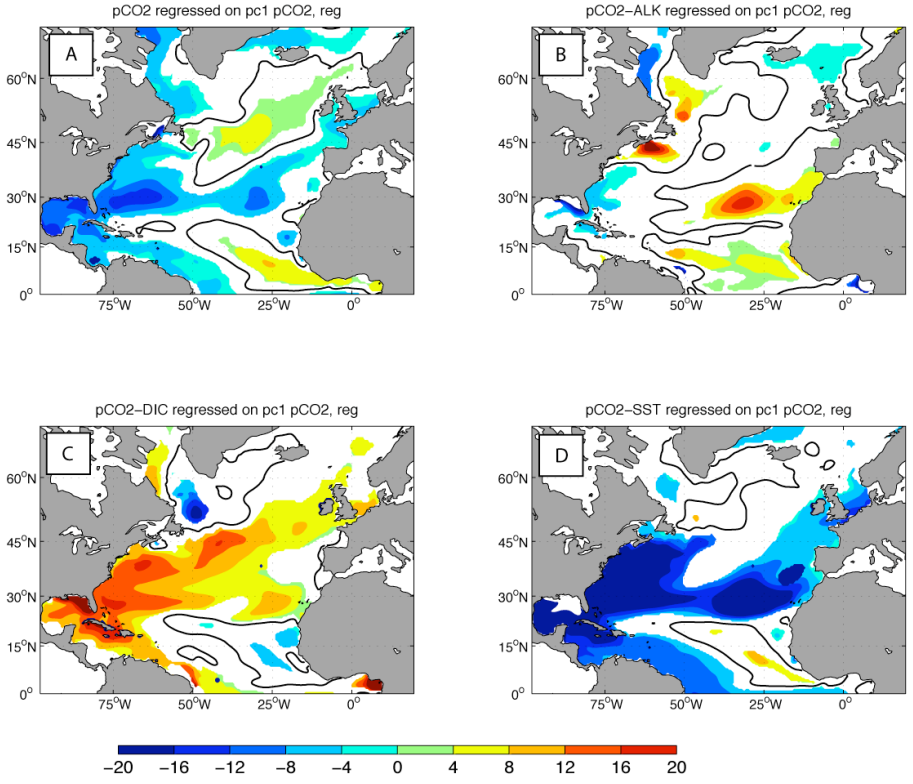

Figure 16. Regression of (a) total pCO_2, (b) pCO_2-ALK, (c) pCO_2-DIC, and (d) pCO_2-SST onto the first principal component of pCO_2 (see Figure 9). Units are in µatm per 1 standard deviation of the PC1. pCO_2 fields and components are detrended and smoothed. Colored areas indicate regions were the correlation coefficient is significantly different from zero at the 95% confidence level. Note: plot (a) is, by definition, the same as the first Empirical Orthogonal Function (EOF1).

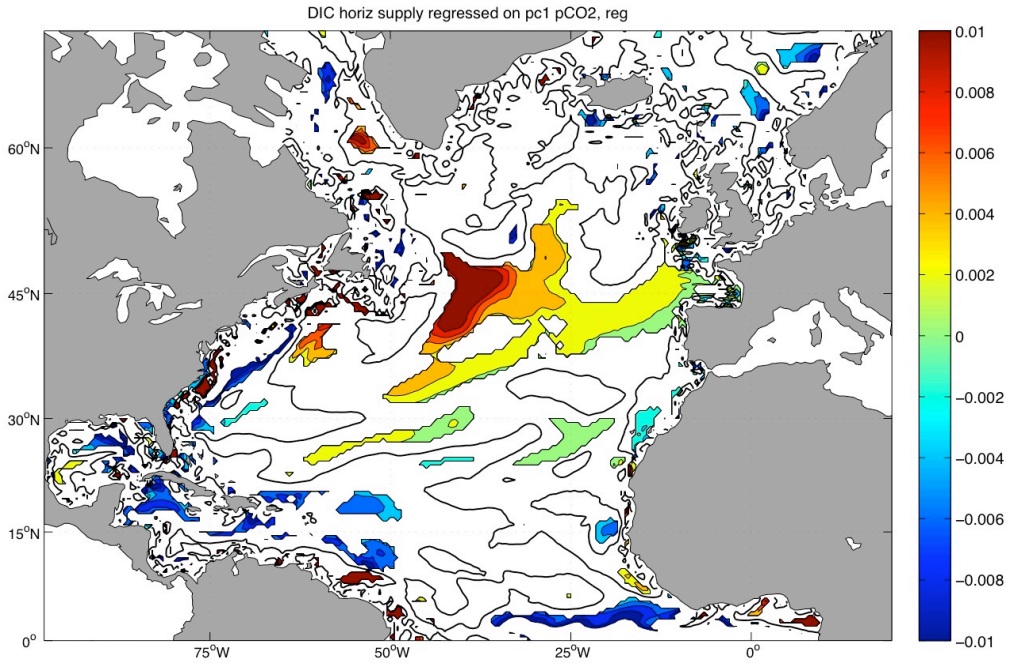

Figure 17. Regression of detrended and smoothed DIC horizontal supply (depth-weighted average over top 100m) onto the first principal component of the pCO_2. Units are in mol/m^3 per 1σ of PC1. Colored areas indicate regions were the correlation coefficient is significantly different from zero at the 95% confidence level.

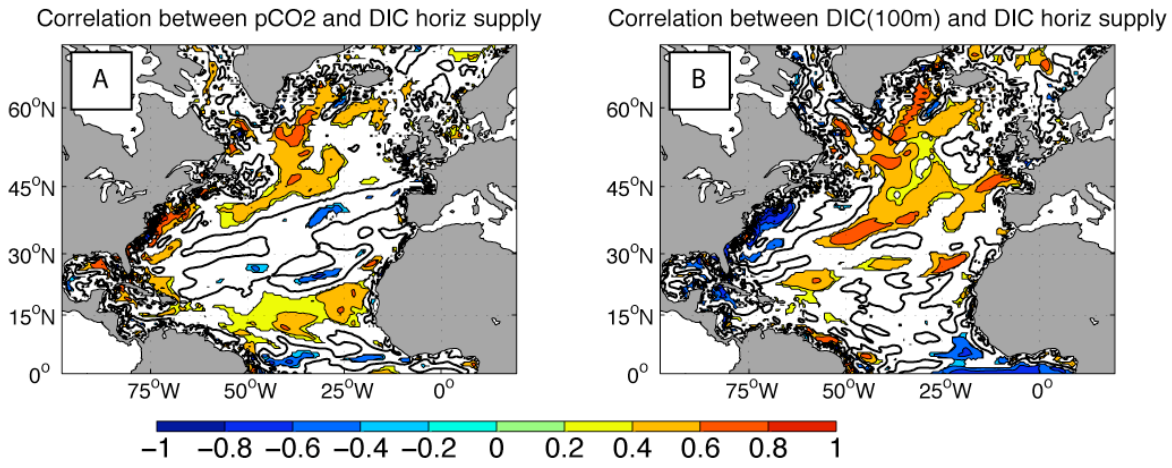

Figure 18. Correlation between (a) pCO_2 and DIC horizontal supply (b) DIC, depth-weighted average over top 100m, and DIC horizontal supply. All fields are detrended and smoothed. Colored areas indicate regions were the correlation coefficient is significantly different from zero at the 95% confidence level.